Circulation Research

ORIGINAL RESEARCH

RBPMS2 Is a Myocardial-Enriched Splicing Regulator Required for Cardiac Function

Alexander A. Akerberg, Michael Trembley, Vincent Butty, Asya Schwertner, Long Zhao, Manu Beerens, Xujie Liu, Mohammed Mahamdeh, Shiaulou Yuan, Laurie Boyer, Calum MacRae, Christopher Nguyen, William T. Pu, Caroline E. Burns, C. Geoffrey Burns

BACKGROUND: RBPs (RNA-binding proteins) perform indispensable functions in the post-transcriptional regulation of gene expression. Numerous RBPs have been implicated in cardiac development or physiology based on gene knockout studies and the identification of pathogenic RBP gene mutations in monogenic heart disorders. The discovery and characterization of additional RBPs performing indispensable functions in the heart will advance basic and translational cardiovascular research.

METHODS: We performed a differential expression screen in zebrafish embryos to identify genes enriched in *nkx2.5*-positive cardiomyocytes or cardiopharyngeal progenitors compared to *nkx2.5*-negative cells from the same embryos. We investigated the myocardial-enriched gene RNA-binding protein with multiple splicing (variants) 2 [*RBPMS2*)] by generating and characterizing *rbpms2* knockout zebrafish and human cardiomyocytes derived from *RBPMS2*-deficient induced pluripotent stem cells.

RESULTS: We identified 1848 genes enriched in the *nkx2.5*-positive population. Among the most highly enriched genes, most with well-established functions in the heart, we discovered the ohnologs *rbpms2a* and *rbpms2b*, which encode an evolutionarily conserved RBP. Rbpms2 localizes selectively to cardiomyocytes during zebrafish heart development and strong cardiomyocyte expression persists into adulthood. Rbpms2-deficient embryos suffer from early cardiac dysfunction characterized by reduced ejection fraction. The functional deficit is accompanied by myofibril disarray, altered calcium handling, and differential alternative splicing events in mutant cardiomyocytes. These phenotypes are also observed in RBPMS2-deficient human cardiomyocytes, indicative of conserved molecular and cellular function. RNA-sequencing and comparative analysis of genes mis-spliced in RBPMS2-deficient zebrafish and human cardiomyocytes uncovered a conserved network of 29 ortholog pairs that require *RBPMS2* for alternative splicing regulation, including *RBFOX2*, *SLC8A1*, and *MYBPC3*.

CONCLUSIONS: Our study identifies *RBPMS2* as a conserved regulator of alternative splicing, myofibrillar organization, and calcium handling in zebrafish and human cardiomyocytes.

GRAPHIC ABSTRACT: A graphic abstract is available for this article.

Key Words: alternative splicing ■ human induced pluripotent stem cells ■ myocytes, cardiac ■ RNA-binding proteins ■ zebrafish

In This Issue, see p 949 | Meet the First Author, see p 950 | Editorial, see p 1001

Cardiomyocytes are the workhorse cells of the heart, producing rhythmic contractions that propel blood through the pulmonary and systemic circulations to achieve organ and tissue perfusion.[1] Cardiomyocyte contraction is the culmination of several ordered molecular events including membrane depolarization, rapid accumulation of calcium in the sarcoplasm, cross-bridge cycling, and sarcomere shortening.[2] Conversely, cardiomyocyte relaxation depends on sarcoplasmic calcium clearance, cross-bridge dissociation, sarcomere re-elongation, and membrane repolarization.

Correspondence to: Caroline E. Burns, PhD, Division of Basic and Translational Cardiovascular Research, Department of Cardiology, Boston Children's Hospital, Boston, MA, Email caroline.burns@childrens.harvard.edu or C. Geoffrey Burns, PhD, Division of Basic and Translational Cardiovascular Research, Department of Cardiology, Boston Children's Hospital, Boston, MA, Email geoff.burns@childrens.harvard.edu

Supplemental Material is available at https://www.ahajournals.org/doi/suppl/10.1161/CIRCRESAHA.122.321728.

For Sources of Funding and Disclosures, see page 997.

Novelty and Significance

What Is Known?

- Alternative pre-mRNA splicing is a fundamental mechanism of post-transcriptional gene regulation that creates lineage-specific functional diversity in the proteome.
- Although heart-specific alternative splicing events are known to ensure the establishment or maintenance of cardiac function, the essential regulatory factors remain incompletely characterized.
- RBPMS2 (RNA-binding protein with multiple splicing [variants] 2) is an RNA-binding protein expressed selectively in the myocardium, but its function was not previously explored through genetic loss-of-function studies.

What New Information Does This Article Contribute?

- We report that human cardiomyocytes or zebrafish embryos devoid of *RBPMS2* suffer from sarcomere organization, calcium handling, and cardiac function defects.
- We also demonstrate that *RBPMS2*-knockout cells or embryos mis-splice several genes, many of which are known to be involved in sarcomere structure, calcium handling, or cardiac function.
- We discovered that a conserved network of orthologous genes in both species relies on RBPMS2 for alternative splicing regulation in cardiomyocytes.

Our collective understanding of the natural mechanisms that support and safeguard cardiac function remains incomplete. We describe a new and essential genetic regulatory mechanism for ensuring robust ventricular myocardial function. The importance of this regulatory mechanism is evident in the conservation of several RBPMS2 splicing targets, which have persisted in humans and zebrafish despite 450 million years of evolutionary divergence. Further research on RBPMS2 and other cardiac-enriched splicing factors will highlight novel opportunities for diagnosing, preventing, and treating heart disease.

Nonstandard Abbreviations and Acronyms

ALPM	anterior lateral plate mesoderm
ASE	alternative splicing event
DKO	double knockout
hiPSC-CM	human induced pluripotent stem cell–derived cardiomyocyte
RBP	RNA-binding protein
rMATS	replicate multivariate analysis of transcript splicing
RRM	RNA recognition motif

Optimal cardiomyocyte physiology is paramount to vertebrate animal fitness. Alterations in cardiomyocyte function stemming from inherited or de novo mutations,[3–5] or environmental exposures to cardiotoxins such as cancer-related treatments and alcohol,[6,7] are frequent causes of primary cardiomyopathies in the pediatric and adult populations. Through the identification of cardiomyopathy-causing mutations and fundamental studies involving genetically engineered cells or animal models, much is already known about the gene activities required for establishing, maintaining, and safeguarding cardiomyocyte function. However, the catalog of genes with documented and indispensable functions in human cardiomyocytes remains incomplete. This is evident when considering that a significant percentage of familial cardiomyopathies lack a genetic diagnosis because the underlying mutations exist in essential but unknown genes or regulatory sequences outside of clinically recognized cardiomyopathy loci.[8] Expanding the catalog of known genes with essential functions in human cardiomyocytes will identify novel candidate loci, biomarkers, and treatment opportunities for cardiomyopathies.

RBPs (RNA-binding proteins) facilitate 5′ capping, splicing, polyadenylation, subcellular localization, stability, and translational efficiency of messenger RNAs.[9] Disruptions to RBP function can cause broad and profound defects in post-transcriptional RNA processing that compromise cellular health and function. Accordingly, numerous monogenic diseases in the human population, including some heart diseases (see below), are caused by damaging mutations in RBP genes.[10]

Using RNA interactome capture, 2 laboratories recently purified hundreds of RBPs from cultured or primary rodent cardiomyocytes,[11,12] many of which were cardiomyocyte-specific, suggesting that they perform specialized functions in heart muscle. Among those identified were several RBPs with previously documented roles in cardiomyocytes, primarily as mediators of alternative splicing, which dictate the properties of target RNAs and the activities of encoded proteins based on exon composition.[13] One such splicing regulator, RBM24 (RNA-binding motif protein 24), is a cardiomyocyte-enriched RBP required for alternative splicing of several sarcomere genes, including *TTN* (titin) and *ACTN2* (actinin alpha 2).[14–17] In the absence of RBM24, sarcomeres fail to form or be maintained leading to cardiomyocyte and cardiac dysfunction.

Another RBP, QKI (quaking), performs a similar role in supporting sarcomere formation and cardiomyocyte contractility by regulating alternative splicing of sarcomere genes, including *ACTN2*.[18] The cardiomyocyte-enriched RBM20 (RNA-binding motif 20) protein acts predominantly as a splicing repressor to exclude specific exons of several genes from mature mRNAs, including *TTN*.[19–22] Missense mutations in *RBM20* cause familial DCM, features of which are recapitulated in genetically engineered pigs[22] and hiPSC-CMs (human induced pluripotent stem cell-derived cardiomyocytes).[19] Of note, in addition to defects in pre-mRNA processing, *RBM20* mutations also induce the accumulation of sarcoplasmic ribonucleoprotein granules, which are likely to contribute to disease pathogenesis in a pleiotropic fashion.[19,22]

Newborns with hypoplastic left heart syndrome (HLHS) were found to carry de novo mutations in the RBP gene *RBFOX2* (RNA binding Fox-1 homolog 2).[23] Cardiomyocyte-specific ablation of *RBFOX2* in the mouse embryo induced a structural heart defect with some features of HLHS. The authors also documented differential alternative splicing of a gene network, including 2 genes that regulate RhoGTPase cycling.[24] In the postnatal heart, expression of *RBFOX2* in cardiomyocytes protects the heart from dilated cardiomyopathy by regulating alternative splicing of numerous genes and transcription of mir-34a.[25,26] Moreover, misexpression of aberrant *RBFOX2* isoforms contributes to heart disease in the context of diabetes and myotonic dystrophy.[27,28] The related cardiomyocyte-enriched RBP gene *RBFOX1* regulates alternative splicing of a network of genes, including *MEF2* (myocyte enhancer factor 2) family members, and confers protection from pressure overload-induced hypertrophic cardiomyopathy in mice.[29]

Lastly, the RBP genes *CELF1* (CUGBP elav-like family member 1) and *MBNL* (muscleblind-like splicing regulator 1) are reciprocally down and upregulated, respectively, in the hearts of neonatal mice to regulate a fetal-to-adult transition in the alternative splicing of numerous genes including many important for vesicular trafficking.[30–34] Differential alternative splicing between fetal and adult hearts in humans has also been reported.[35] Taken together, these studies underscore the essential and dynamic nature of alternative splicing regulation in cardiomyocytes, which supports cardiomyocyte physiology and protects the heart from dysfunction over the life of a vertebrate animal.

The founding member of the conserved RNA-binding protein with multiple splicing (variants) 2 *(RBPMS2)* gene family was discovered in a differential expression screen designed to identify cardiac-enriched transcripts in *Xenopus laevis*[36] (reviewed in Akerberg et al[37]). The encoded protein contains an RRM and binds directly to RNA.[38] In situ hybridization confirmed strong enrichment of *RBPMS2* expression in cardiomyocytes of amphibian and avian embryos.[36,39] Enriched expression of *RBPMS2* has since been reported in the zebrafish embryonic heart[40] and in human cardiomyocytes profiled by single-cell RNA sequencing (Single Cell Type Atlas).[41] The consistent enrichment of *RBPMS2* expression in vertebrate hearts is suggestive of a specialized and essential function in cardiomyocytes, but this hypothesis has yet to be explored through gene knockout studies.[37]

Here, we describe the first genetic loss-of-function study designed to explore the role of *RBPMS2* in zebrafish and hiPSC-CMs. Specifically, we show that *rbpms2*-deficient zebrafish embryos suffer from cardiac dysfunction characterized by reduced ejection fraction. The functional deficit is accompanied by myofibrillar disarray and calcium handling defects in mutant cardiomyocytes. *rbpms2*-deficient animals also exhibit differential alternative splicing of 150 genes, including several responsible for sarcomere structure and calcium handling. Lastly, *RBPMS2*-deficient human cardiomyocytes display virtually identical cellular phenotypes and share a conserved network of 29 mis-spliced genes with *rbpms2*-deficient zebrafish. Ultimately, our study identifies a novel and conserved RBP that is indispensable for the health and function of cardiomyocytes.

METHODS

Data Availability

All data and materials will be made publicly available upon publication. RNA-sequencing datasets were deposited into the NCBI (National Center for Biotechnology Information) gene expression omnibus (GEO) repository under accession numbers GSE167416, GSE167414, and GSE207681. Please see the Major Resources Table in the Supplemental Materials.

Zebrafish Husbandry and Strains

Zebrafish were bred and maintained following animal protocols approved by the Institutional Animal Care and Use Committees at Massachusetts General Hospital and Boston Children's Hospital. All protocols and procedures followed the guidelines and recommendations outlined by the Guide for the Care and Use of Laboratory Animals. The following zebrafish strains were used in this study: *TgBAC(-36nkx2.5:ZsYellow)*^{fb7},[42] *Tg(myl7:GFP)*^{fb1} [formerly *Tg(cmlc2:GFP)*^{fb1}*],*[43] *Tg(myl7:NLS-eGFP)*^{fb18} [formerly *Tg(cmlc2:nucGFP)*^{fb18}*],*[44] *Tg(myl7:actn3b-EGFP)*^{sd10} [formerly *Tg(cmlc2:actinin3-EGFP)],*[45] *rbpms2a*^{chb3} (this study), and *rbpms2b*^{chb4} (this study).

Generation and Genotyping of *rbpms2a*^{ch3} and *rbpms2b*^{ch4} Mutant Alleles

Customized TALENs (transcription activator-like effector nucleases)[46–48] were used to induce double-stranded breaks in regions of the *rbpms2a* and *rbpms2b* loci that encode the RMM (RNA-recognition motifs). TALENs were designed to bind the sequences 5′- TGCCTGTTGACATCAAGC-3′ (+) and 5′-TTGAAGGGTCTGAACAGC-3′ (—) in exon 2 of *rbpms2a* and 5′- TGCCAACAGATATCAAAC-3′ (+) and 5′-TTAAATGGTCGAAATAGC-3′ (—) in exon 2 of *rbpms2b*. TALEN constructs were constructed as described (Sanjana

et al., 2012). Messenger RNAs encoding each TALEN pair were produced in vitro and co-injected into one-cell stage zebrafish embryos as described.[46] Germline transmission of TALEN-induced mutations were detected using fluorescent polymerase chain reaction (PCR) and DNA-fragment analysis as described.[49] The nucleotides deleted in the mutant alleles *rbpms2a*^{chb3} and *rbpms2b*^{chb4} are shown (Figure S4A and S4B). The primers utilized to distinguish wild-type *rbpms2a* and *rbpms2b* from the mutant alleles *rbpms2a*^{chb3} and *rbpms2b*-^{chb4} by fluorescent PCR and DNA-fragment analysis are also shown (Figure S8). The wild-type alleles produce amplicons of 97 base pairs (bp)(*rbpms2a*) and 76bp (*rbpms2b*), whereas the mutant alleles produce amplicons of 83bp (*rbpms2a*^{chb3}) and 74bp (*rbpms2b*^{chb4}).

hiPSC Maintenance and Genome Editing

All hiPSC lines were maintained at 37 °C, 5% CO_2 in Essential 8 medium (catalog no. A1517001, Thermo Fisher Scientific) and passaged every 3 to 4 days using Versene (catalog no. 15040066, Thermo Fisher Scientific). Culture dishes were precoated with 0.5% GelTrex matrix solution (catalog no. A1413302, Thermo Fisher Scientific). CRISPR/Cas9 genome editing was performed to create isogenic lines. Briefly, guide RNA for *RBPMS2* (sequence 5′-GTCTTGCAGTGAGCTTGATC-3′) was synthesized using the T7 MegaShortScript transcription kit (Thermo Fisher Scientific). We previously described methods[50] to generate a doxycycline-inducible Cas9 line in the WTC-11 iPSC background (Coriell Institute). Targeted integration of Cas9 into the AAVS1 (adeno-associated virus integration site 1) locus was performed using Addgene plasmids no. 73500 and no. 48139. This WTC-11 AAVS1$^{Cas9/+}$ hiPSC line was treated with doxycycline (2 µg/mL) for 16 hours before transfection to induce expression of an nuclear localization sequence (NLS)-SpCas9 fusion protein. After induction, ≈0.5×10^6 cells were transfected with 10 µg guide RNA using an Amaxa nucleofector (Lonza Technologies). Cells were seeded at a low density to pick single clones. Positive clones were confirmed by Sanger and amplicon sequencing. Stem cell marker expression was validated in isolated cell lines by flow cytometry using anti-SSEA4 (stage-specific embryonic antigen 4)-FITC (catalog no. 130-098-371, Miltenyi Biotec) and anti-IgG-FITC (catalog no. 130-104-611, Miltenyi Biotec) for negative control. Normal karyotypes were confirmed for both wild-type control and *ΔRBPMS2* hiPSCs by KaryoStat (Thermo Fisher).

RESULTS

Enriched Expression of the RBP Genes *rbpms2a* and *rbpms2b* in Zebrafish Cardiomyocytes

Lineage-enriched genes often perform specialized and essential functions in the development, maintenance, or function of the cell populations they mark. To generate a candidate list of zebrafish genes with essential activities in cardiopharyngeal progenitors or embryonic cardiomyocytes, we sought to identify mRNAs with restricted expression to the subset of anterior lateral plate mesodermal (ALPM) cells marked by the *nkx2.5:ZsYellow* transgene. This population contains cardiopharyngeal progenitors for multiple cell types including second heart field-derived ventricular cardiomyocytes and outflow tract lineages, a subset of pharyngeal muscles, and endothelium of the pharyngeal arch arteries.[42,51–55] It also contains early-differentiating ventricular cardiomyocytes derived from the first heart field.[51,53,54]

To isolate ALPM cells labeled with the transgene, *Tg(nkx2.5:ZsYellow)* embryos were dissociated into single cells at a developmental stage when ZsYellow fluorescence is restricted to the ALPM (14–16 somites stage; Figure 1A). Dissociated cells were separated by fluorescence-activated cell sorting into ZsYellow-positive and ZsYellow-negative subpopulations before being subjected to RNA-sequencing and differential expression analysis (Figure 1A; Figure S1A through S1C). From this, we identified 1848 protein-coding RNAs enriched in the ZsYellow-positive population (Figure 1A; Table S1) after applying the inclusion criteria for Gene Ontology (GO) term enrichment analysis (| fold change [FC] | >1.5; adjusted *P* value [*P* adj]<0.05). Low replicate numbers precluded us from making claims of statistical significance based on the reported *P* values (Table S1). As a result, this gene set is ranked based on log2FC (Figure S1D, Table S1). Nonetheless, among the enriched genes were several previously characterized lateral plate mesodermal markers that encode transcription factors essential for cardiopharyngeal development including *nkx2.5*, *hand2*, *gata4/5/6*, *mef2ca/b*, *tbx1/5a/20*, *isl1*, and *fgf8a/10a/10b* (Figure S1D; Table S1). Due to the presence of early-differentiating cardiomyocytes in the ZsYellow-positive population, we also identified numerous genes encoding sarcomere components (*cmlc1*, *myl7* [*cmlc2*], *myh7* [*vmhc*], *myh6* [*amhc*], *acta1b*, *actc1a*, *actn2b*, *tnni1b*, *tnnt2a, tnnc1a, tpm4a, ttn.2*), calcium handling proteins (*slc8a1a* [*ncx1*], *ryr2b, atp2a2a* [*serca2*]), and other factors expressed preferentially in cardiomyocytes (*cx36.7*, *nppa/al/b*; Figure S1D; Table S1). As expected, GO term enrichment analysis uncovered overrepresentation of biological process terms "heart development," "angiogenesis," "heart contraction," "actin cytoskeletal organization," and "sarcomere organization" in the ALPM-enriched gene set (Figure S1E, see Table S1 for complete GO term analysis). The successful identification of ALPM markers with well-documented and indispensable roles in cardiopharyngeal progenitors or cardiomyocytes suggests that novel molecular activities of equal importance are likely to be among the uncharacterized ALPM-restricted genes.

The RBP genes *rbpms2a* and *rbpms2b* stood out among the most highly enriched as having never been implicated in heart development or function (Figure S1D; Table S1). Furthermore, of the 19 ALPM-enriched genes that were annotated with GO terms "RNA processing" and "RNA binding," *rbpms2a* was the most highly enriched (≈14-fold enrichment), and *rbpms2b*

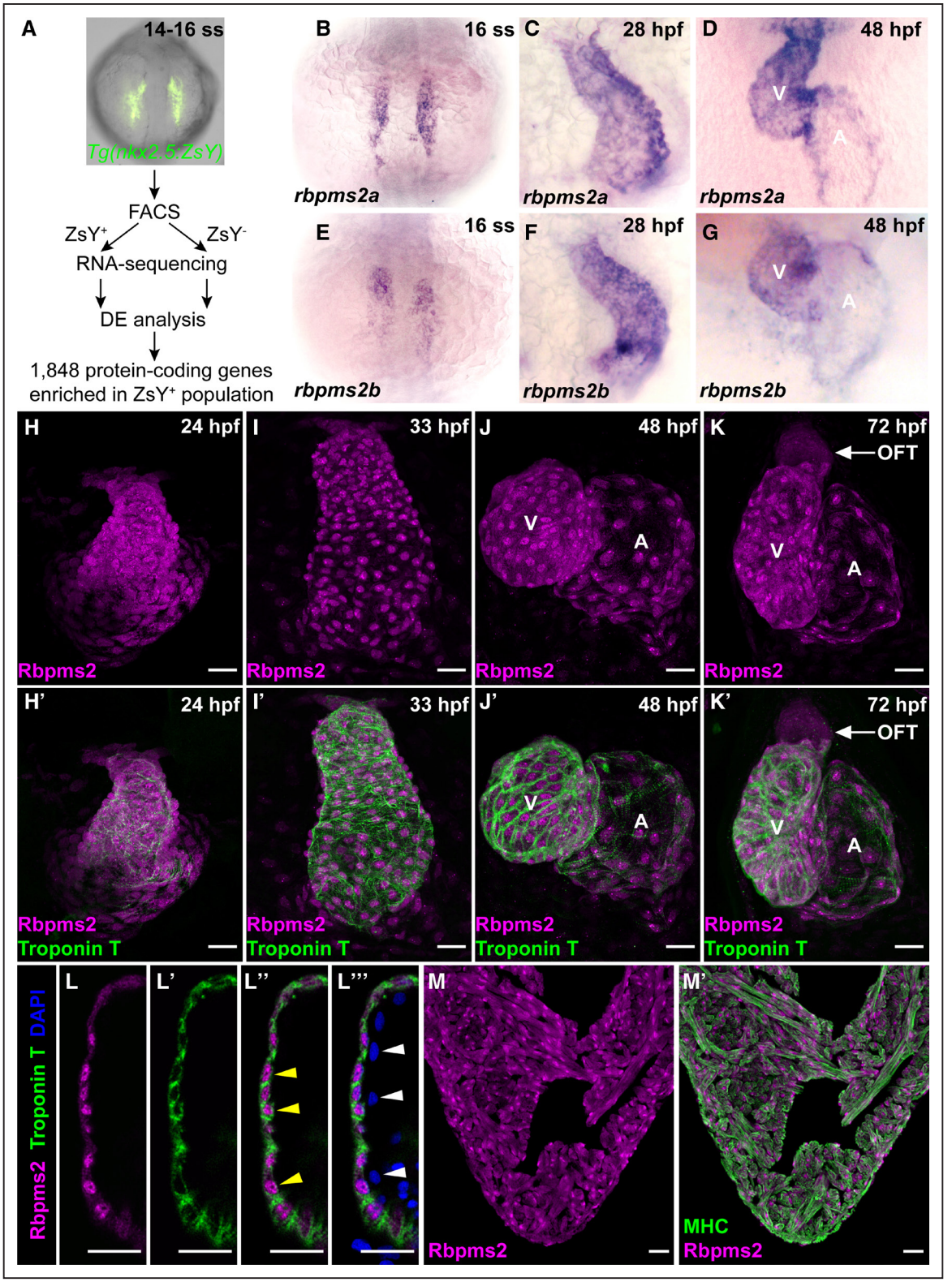

Figure 1. Restricted expression of RNA-binding proteins Rbpms2a (RNA-binding protein with multiple splicing [variants] 2a) and Rbpms2b to the zebrafish myocardium.

A, Workflow used to identify 1848 protein-coding RNAs enriched in ZsYellow-positive (ZsY+) cardiopharyngeal progenitors or cardiomyocytes of the anterior lateral plate mesoderm in comparison to ZsYellow-negative (ZsY−) cells from the same 14–16 somites stage (ss) *Tg(nkx2.5:ZsYellow)* embryos. **B**–**G**, Representative brightfield images of 16 ss (**B** and **E**), 28 hours postfertilization (hpf; **C** and **F**), and 48 hpf (**D,G**) embryos processed for in situ hybridization with riboprobes that detect *rbpms2a* (**B**–**D**) or *rbpms2b* (**E**–**G**). n=10/group. **H**–**K**′, Representative confocal projections of hearts in 24 hpf (**H** and **H**′), 33 hpf (**I** and **I**′), 48 hpf (**J** and **J**′), and 72 hpf (**K** and **K**′) zebrafish embryos (*Continued*)

(≈5-fold enrichment) ranked sixth based on log2FC (Figure S1F; Table S1). Classified as ohnologs, *rbpms2a* and *rbpms2b* encode proteins that are 92% identical (96% in the RRM; Figure S2A and S2B) and perform redundant functions in oocyte differentiation.[40] Full-length Rbpms2a and Rbpms2b share >81% identity with human RBPMS2 (Figure S2A and S2B), and their RRM domains are over 92% identical (Figure S2A and S2B). Such a high degree of sequence conservation suggests that the molecular function of RBPMS2 proteins and the properties of their binding motifs are also likely to be conserved across evolution.

To validate the predicted ALPM localization of *rbpms2a* and *rbpms2b,* we performed in situ hybridization for both genes at the same developmental stage (16 somites stage) used for profiling *nkx2.5:ZsYellow*-positive ALPM cells (Figure 1A). As anticipated, both transcripts localized bilaterally to the ALPM (Figure 1B and 1E), in a pattern mirroring early-differentiating cardiomyocytes at this stage.[56] Later-stage analysis localized *rbpms2a* and *rbpms2b* to the linear heart tube at 24 to 28 hours postfertilization (hpf; Figure 1C and 1F; Figure S3A and S3C) and to both the atrium and ventricle at 48 hpf (Figure 1D and 1G; Figure S3B and S3D). Consistent with previous reports,[40,57] extra-cardiac expression was observed in the pronephric duct and retina (Figure S3A through S3D).

To investigate the lineage specificity and subcellular localization of Rbpms2a and Rbpms2b in the zebrafish heart, we immunostained wild-type embryos with a monoclonal antibody raised against human RBPMS2, which cross-reacts with zebrafish Rbpms2 (see below). Consistent with the distribution of *rbpms2a/b* transcripts, Rbpms2 protein was detected in the heart tube (Figure 1H and 1I; Figure S3E and S3F), 2-chambered heart (Figure 1J and 1K; Figure S3G), pronephric duct (Figure S3E through S3G), and retina (Figure S3F and S3G). Double-immunostaining for Rbpms2 and the myocardial marker cardiac troponin T (CT3 antibody) revealed that Rbpms2 localizes to the myocardium at all stages analyzed (Figure 1H′, I′, J′, and K′). Examination of single optical sections through the ventricular wall showed nuclear Rbpms2 signals surrounded by troponin T–positive cytoplasm, confirming myocardial localization (Figure 1L through 1L‴). Adjacent endocardial cells were devoid of Rbpms2 signals, demonstrating that expression in the ventricular chamber is restricted to the myocardial layer (Figure 1L through 1L‴). Weak expression of Rbpms2 also became evident in the outflow tract by 72 hpf (Figure 1K and 1K′). The subcellular distribution of Rbpms2 appeared variable, ranging from a nucleocytoplasmic distribution to exclusively nuclear (Figure 1H, 1I, 1J, and 1K), but the significance of this observation is unknown. Lastly, we documented Rbpms2 expression, both nuclear and cytoplasmic, in cardiomyocytes of adult zebrafish (Figure 1M and M′), suggesting that Rbpms2 functions in the myocardium continuously throughout the lifespan of zebrafish rather than transiently during embryogenesis.

Generation of *rbpms2*-Null Zebrafish

To determine if *rbpms2a* and *rbpms2b* are required for myocardial development or cardiac function, we created mutant alleles of both genes using TALENs.[47] TALEN pairs were designed to target DNA sequences encoding N-terminal regions of the RRM domains (Figure S4A and S4B). We isolated the mutant alleles *rbpms2a*^{chb3} and *rbpms2b*^{chb4}, which carry frame-shifting deletions and premature stop codons that truncate the proteins by >80% (Figure 2A and 2B; Figure S4A and S4B). The truncations also remove 82% of the RRMs, suggesting that the RNA-binding activities of the mutant proteins are abolished or significantly compromised. As a result, both alleles are likely to be null. Animals homozygous for either *rbpms2a*^{chb3} or *rbpms2b*^{chb4} are grossly indistinguishable from siblings during all life stages, which is consistent with a previous study that independently generated mutant alleles of *rbpms2a* and *rbpms2b*.[40]

To determine if *rbpms2a* and *rbpms2b* perform redundant functions in the heart, we generated and examined double homozygous embryos (ie, *rbpms2a*$^{chb3/chb3}$; *rbpms2b*$^{chb4/chb4}$ animals) for cardiac defects. Double knockout (DKO) animals are grossly indistinguishable from control siblings for the first ≈30 hours of life, including normal *nkx2.5* expression in the ALPM (Figure S4C through S4E). By ≈33 hpf, they develop a characteristic indentation of the yolk (Figure S4F and S4G), which is indicative of mild pericardial edema. At this stage, double mutants are delayed in initiating blood flow although peristalsis of the heart tube is readily evident. By 72 hpf, pericardial edema is markedly more severe (Figure 2C and 2D), suggesting that *rbpms2*-null animals suffer from a cardiac malformation or ongoing functional deficit. This phenotype is observed specifically in double-mutant animals, demonstrating that

Figure 1 Continued. coimmunostained with antibodies that detect Rbpms2 (magenta) or cardiac troponin T (CT3 antibody; green). Single (**H**, **I**, **J**, and **K**) and merged double channel (**H′**, **I′**, **J′**, and **K′**) images are shown. n=10/group. **L**–**L‴**, Single optical section through the ventricular wall of a 48 hpf embryo coimmunostained with antibodies that detect Rbpms2 (magenta) or cardiac troponin T (green) and counterstained with DAPI (4',6-diamidino-2-phenylindole; blue). Single (**L** and **L′**), merged double (**L″**), and merged triple (**L‴**) channel images are shown. Yellow arrowheads highlight Rbpms2-positive cardiomyocyte nuclei surrounded by troponin T–positive cytoplasm. White arrowheads highlight Rbpms2-negative nuclei in adjacent endocardial cells lining the ventricular chamber. n=4. **M** and **M′**, Representative confocal projections of a histological section through the ventricle of an adult zebrafish heart coimmunostained with antibodies that detect Rbpms2 (magenta) or MHC (myosin heavy chain; MF20 antibody; green). Single channel (**M**) and merged double channel (**M′**) images are shown. n=18 sections, 6 from each of 3 hearts. Scale bars=25 μm. A indicates atrium; DE, differential expression; FACS, fluorescence-activated cell sorting; OFT, outflow tract; and V, ventricle.

ORIGINAL RESEARCH

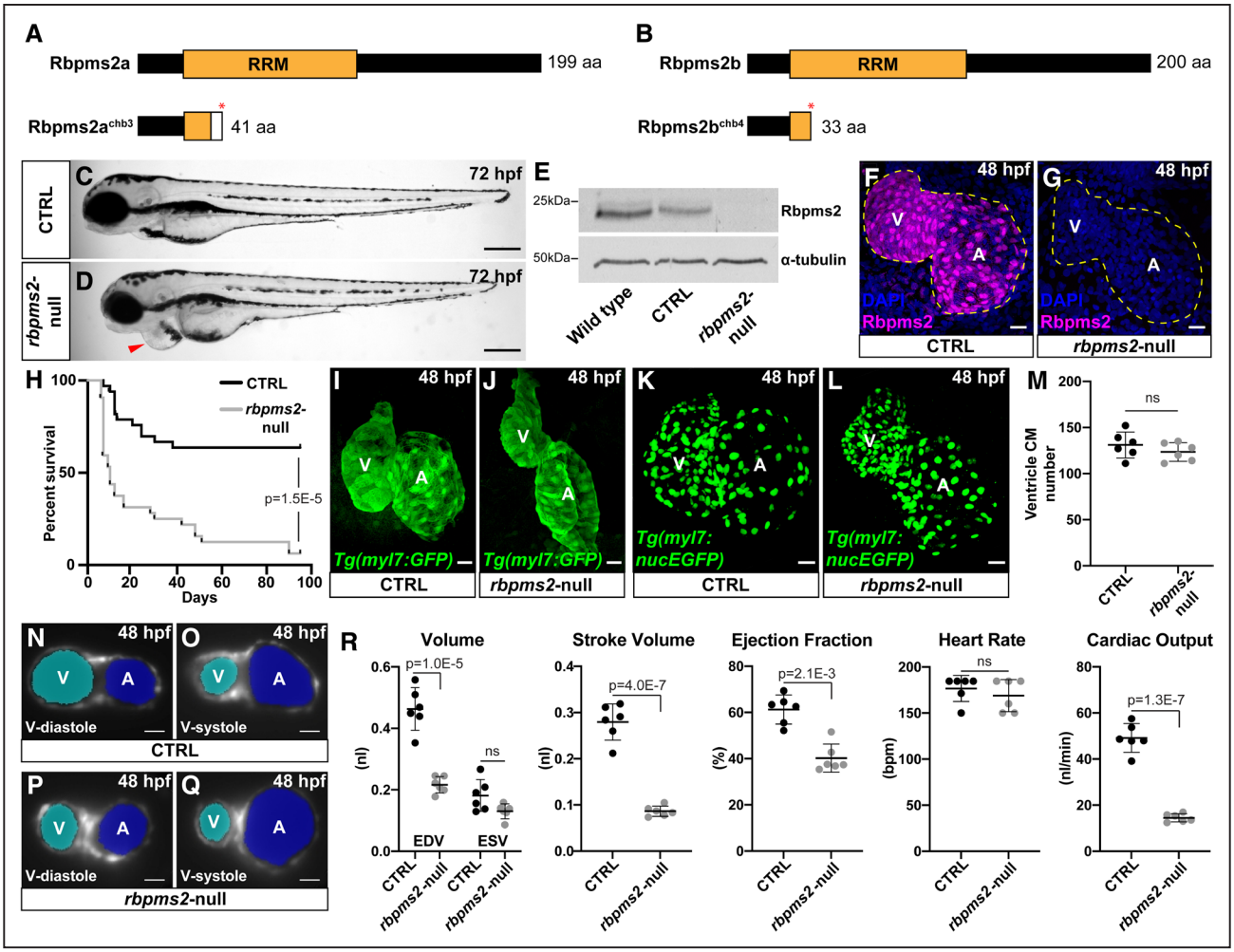

Figure 2. *rbpms2a* and *rbpms2b* are required redundantly for ventricular function in zebrafish.
A and **B**, Schematic diagrams of the zebrafish Rbpms2a and Rbpms2b proteins (**top**) and the predicted protein products of the *rbpms2a*^{chb3} and *rbpms2b*^{chb4} mutant alleles (**bottom**). The asterisks (*) mark the locations of premature stop codons within the RRMs (RNA-recognition motifs) caused by frame-shifting deletions. The white box in (**A**) shows the location of divergent amino acids before the stop codon. **C** and **D**, Representative brightfield images of control-sibling (**C**; CTRL) and *rbpms2*-null (*rbpms2a*$^{chb3/chb3}$; *rbpms2b*$^{chb4/chb4}$; **D**) embryos at 72 hours postfertilization (hpf). Arrowhead highlights pericardial edema in the mutant. n=50/group. Scale bars=250µm. **E**, Western blot showing Rbpms2 levels in 48 hpf wild-type (WT), CTRL, and *rbpms2*-null embryos (**top**) relative to the loading control alpha-tubulin (**bottom**). **F** and **G**, Representative confocal projections of hearts in 48 hpf CTRL (**F**) and *rbpms2*-null (**G**) embryos immunostained with an anti-Rbpms2 antibody (magenta) and counterstained with DAPI (4',6-diamidino-2-phenylindole; blue). The dotted lines delineate the myocardium as ascertained from the Rbpms2 signal (**F**) or *Tg(myl7:eGFP)* reporter signal present in these animals (**G**; not shown). n=15/group. **H**, Kaplan-Meier plot for CTRL (n=33) and *rbpms2*-null (n=33) animals. Statistical significance was determined using a log-rank test. The significant *P* value is shown. **I**–**L**, Representative confocal projections of hearts in 48 hpf CTRL (**I** and **K**) or *rbpms2*-null (**J** and **L**) embryos carrying the *myl7:GFP* (**I**,**J**; n=10/group) or *myl7:nucGFP* (**K** and **L**) transgenes immunostained with an anti- GFP (green fluorescent protein) antibody. **M**, Dot plot showing ventricular cardiomyocyte (CM) numbers in CTRL (n=6) and *rbpms2*-null (n=6) hearts at 48 hpf. Error bars show one standard deviation. Statistical significance was determined by an unpaired, 2-tailed Student's *t* test assuming equal variances. **N**–**Q**, Representative single-plane light sheet fluorescence microscopy images of hearts in 48 hpf CTRL (**N** and **O**) and *rbpms2*-null (**P** and **Q**) embryos carrying the *myl7:GFP* transgene. Images of hearts during ventricular diastole (**N** and **P**) or systole (**O** and **Q**) are shown with Cardiac Functional Imaging Network (CFIN) overlays of the atrial (blue) and ventricular (cyan) lumens. **R**, Dot plots showing end-diastolic volumes (EDV) and end-systolic volumes (ESV), stroke volumes, ejection fractions, heart rates, and cardiac outputs of ventricles in 48 hpf CTRL (n=6) and *rbpms2*-null (n=6) animals measured with CFIN. Error bars show one SD. Statistical significance was determined by Mann-Whitney *U* test or an unpaired, 2-tailed Student's *t* test assuming equal variances. Significant *P* values are shown. Scale bars=25 µm. A indicates atrium; aa, amino acid; ns, not significant; and V, ventricle.

rbpms2a and *rbpms2b* perform redundant functions in the heart, as they do in oocytes.[40]

Western blotting and whole-mount immunostaining revealed that the zebrafish epitopes recognized by the anti-human RBPMS2 antibody are completely absent in double mutants (Figure 2E through 2G), demonstrating that the antibody cross-reacts with zebrafish Rbpms2. It also suggests that the mutant mRNAs or proteins are unstable, further suggesting that *rbpms2a*^{chb3} and *rbpms2b*^{chb4} are bona fide null alleles.

To assess double-mutant viability, we monitored the survival of control-sibling and DKO animals from embryonic

stages to adulthood. Over 50% of *rbpms2*-null animals died by 2 weeks of age (Figure 2H). Furthermore, 85% of animals were dead by 60 days postfertilization, and the remaining small percentage of animals did not survive beyond 6 months postfertilization. Independent of age, death was generally preceded by progressive pericardial edema, suggesting that cardiac dysfunction is the underlying cause of premature mortality in *rbpms2*-null animals.

Rbpms2-Deficient Animals Exhibit Cardiac Dysfunction Characterized by Reduced Ejection Fraction

To evaluate DKO embryos for structural heart disease, we examined hearts of 48 hpf control-sibling and *rbpms2*-null animals carrying the *myl7:GFP* transgene, which labels the entire myocardium with GFP (green fluorescent protein). Although the 2-chambered heart in double mutants displayed normal left-right patterning, the ventricle was displaced anteriorly relative to the atrium (Figure 2I and 2J), likely reflecting stretching at the cardiac poles caused by pericardial edema. Atrial size was not overtly different in *rbpms2*-null animals, but their ventricles were smaller by comparison to those in control siblings (Figure 2I and 2J). To determine if this reflected a diminished ventricular cell number, we quantified cardiomyocytes in control-sibling and *rbpms2*-null animals carrying the *myl7:nucGFP* transgene, which labels cardiomyocyte nuclei with GFP. Both ventricular and atrial cardiomyocyte numbers were unaltered in double mutants (Figure 2K through 2M; Figure S5A), demonstrating that any deviations in chamber size are not attributable to altered myocardial cell content. It also suggests that *rbpms2a* and *rbpms2b* are dispensable for cardiomyocyte differentiation from the first and second heart fields, which is the principal method by which cardiomyocytes are produced before 48 hpf in zebrafish.[42,58–60] Ultimately, these data demonstrate that early cardiac morphogenesis is largely unperturbed in double-mutant animals, with the only apparent anatomic abnormality being a reduction in ventricular size. Because mutant ventricles have normal numbers of cardiomyocytes, we can deduce that the ventricular cardiomyocytes themselves are smaller, which is apparent based on the increased density of cardiomyocyte nuclei in mutant ventricles (Figure 2K and 2L).

To evaluate *rbpms2*-null hearts for functional deficits, we measured ejection fraction and cardiac output in 48 hpf animals using our previously described Cardiac Functional Imaging Network.[61] Briefly, we used light sheet fluorescence microscopy to capture dynamic Z-stack images of GFP+ hearts in control-sibling and DKO *myl7:GFP* transgenic embryos over several cardiac cycles. From these data, the Cardiac Functional Imaging Network extracted dynamic chamber volumes over time, including end-diastolic volume (EDV) and end-systolic volume (ESV) as described.[61] Whereas ventricular ESV was unchanged in DKO animals, EDV was significantly reduced (Figure 2N through 2R). As a result, 3 indices of ventricular function, all of which are calculated from EDV and ESV, were also significantly reduced. These include stroke volume SV=EDV-ESV ejection fraction EF=SV/EDV and cardiac output (stroke volume×heart rate; Figure 2R). Heart rate was unchanged in the mutant (Figure 2R). The reduction in EDV is consistent with the diminutive size of the DKO ventricle (Figure 2I through 2L), and the reduced ejection fraction is suggestive of systolic heart failure stemming from compromised cardiomyocyte contraction. Cardiac Functional Imaging Network analysis also revealed an increase in atrial volume (Figure S5B), which was not grossly obvious after fixation (Figure 2I through 2L). This was accompanied by a slight decrease in atrial ejection fraction (Figure S5C). Atrial enlargement is a common secondary consequence of impaired ventricular function.[62] Taken together, these data demonstrate that *rbpms2a* and *rbpms2b* are required for robust ventricular function in the zebrafish embryo. This requirement likely extends beyond embryogenesis, because the longest-living DKO animals exhibit signs of cardiac dysfunction such as stunted growth and pericardial edema (Figure S6A). Examination of cardiac sections from these animals revealed hearts with diminutive and fibrotic ventricles as well as massively enlarged atria (Figure S6B through S6E), suggestive of ongoing ventricular dysfunction and reactive atrial dilation.

Identification of Differential Alternative Splicing Events in *rbpms2*-Null Zebrafish

To identify gene expression changes in *rbpms2*-null embryos, we performed bulk RNA-sequencing and differential expression analysis on control-sibling and *rbpms2*-null animals at 33 hpf, the earliest developmental stage when DKO animals are distinguishable by morphology (Figure S4C and S4D). We reasoned that early-stage analysis would maximize the chances of highlighting primary molecular defects without interference by secondary responses to cardiac dysfunction. Importantly, we confirmed that the primitive ventricles in 33 hpf *rbpms2*-null animals exhibit a functional deficit by documenting reduced myocardial wall movement at the arterial pole of the heart tube (Figure S7A). We also confirmed that total cardiomyocyte numbers are unaltered at 33 hpf in double mutants (Figure S7B), reducing the chances that any changes in gene expression would be attributable to altered cellular composition. Lastly, we profiled whole embryos, instead of purified cardiomyocytes, because of the difficulty in recovering sufficient numbers of healthy, pure cardiomyocytes at this stage by embryo dissociation and fluorescence-activated cell sorting.

Although RNA-sequencing and gene-level differential expression analysis did not identify any dysregulated transcripts in *rbpms2*-null animals (|FC|>1.5; *P* adj<0.05; Figure S8A; Table S2), isoform-level differential expression analysis yielded 105 downregulated and 97 upregulated transcripts (|FC|>1.5; *P* adj<0.05; Figure S8B; Table S3). GO term analysis did not identify overrepresentation of any terms in either gene set (false discovery rate <0.05). However, among the downregulated transcripts, we found three well-characterized myocardial genes including phospholamban (*pln/plna*),[63,64] atrial myosin heavy chain 6 (*myh6*),[65] and natriuretic peptide precursor a ([*nppa*][66,67]; Figure S8B; Table S3). We documented trending downregulation of *nppa* by reverse-transcription quantitative PCR (RT-qPCR) at 33 hpf (Figure S7C). However, this was short-lived because 2 subsequent developmental stages showed statistically significant (48 hpf) or trending (72 hpf) increases in *nppa* expression (Figure S7C), which is characteristic behavior for *nppa* in response to cardiac stress (Becker et al[66]). RT-qPCR analysis of *myh6* revealed a downward trending but statistically insignificant change in double mutants (Figure S7D). Ultimately, downregulation of these genes is unlikely to explain the ventricular phenotype in *rbpms2*-null mutants because *nppa*-null zebrafish do not exhibit any gross cardiac defects[67], and the primary defect in *myh6*-deficient animals is a silent atrium.[65]

Phospholamban is a reversible micropeptide inhibitor of the SERCA2a (Sarco/endoplasmic reticulum calcium ATPase 2a) pump, which removes calcium from the sarcoplasm to facilitate cardiomyocyte relaxation.[63] Mutations in *PLN* cause dilated cardiomyopathy in the human population.[68] Publicly available cDNA sequences and annotations of the *pln* locus in the zebrafish genome (Genome Reference Consortium Zebrafish Build 11 [GRCz11]; Ensembl annotation release 106[69]) suggest that *pln* is alternatively spliced. Interestingly, one of the alternatively spliced isoforms of *pln* (ENSDART00000141159; *pln-203*) was found to be downregulated in *rbpms2*-null animals (FC=−43.00; *P* adj=8.24×10^{-10}; Figure S8B; Table S3). However, 3 additional alternatively spliced *pln* transcripts (ENSDART00000086648, ENSDART00000132012, ENSDART00000133911) were unchanged (Table S3), highlighting the possibility that Rbpms2 functions in the zebrafish myocardium to regulate alternative splicing, a molecular function previously ascribed to the closely related RBPMS protein,[70] but not to RBPMS2 itself.[37]

To investigate this possibility directly, we performed replicate multivariate analysis of transcript splicing (rMATS)[71] on the same RNA-sequencing dataset and identified 166 differential alternative splicing events (ASEs) in 150 total genes in *rbpms2*-null animals (0 uncalled replicates; false discovery rate <0.1; |Incleveldifference|>0.1; Figure 3A and 3B; Table S4). The most common ASE was skipped exon, representing 49% of the total ASEs, followed by alternative 3′ splice site (18%), alternative 5′ splice site (15%), mutually exclusive exons (12%), and retained intron (5%; Figure 3A and 3C; Table S4). In the skipped exon category, ASEs were split relatively evenly between exon inclusion and exon exclusion in *rbpms2*-null embryos (Figure 3C; Table S4). GO term enrichment analysis did not identify overrepresentation of any terms from the differentially spliced genes (false discovery rate <0.05).

Notably, several genes expressed in cardiomyocytes were found to be differentially spliced in *rbpms2*-null animals. They include *mybpc3* (myosin binding protein C3)[72] and *myom2a* (myomesin 2a; Single Cell Type Atlas),[41] both of which encode components of the sarcomere.[73,74] Mutations in *MYBPC3* are common causes of familial hypertrophic cardiomyopathy in the human population.[75] Another mis-spliced myocardial gene was *sslc8a1a* (solute carrier family 8 member 1a; previously named *ncx1* [sodium-calcium exchanger 1]) which encodes a plasma membrane transporter responsible for extruding calcium from cardiomyocytes during cardiac relaxation.[76–78]

In the case of *mybpc3*, exons 2 and exons 10 were identified as cassette exons whose inclusion levels (Inclevels) in mature *mybpc3* transcripts were found to be significantly lower in *rbpms2*-null animals, as evidenced by positive Inclevel differences where Incleveldifference=Inc $\text{level}^{\text{control}}$−$\text{Inclevel}^{\textit{rbpms2}\text{-null}}$ (Figure 3B; Table S4). The same was true for exon 16 of *myom2a* and exon 5 of *slc8a1a* (Figure 3B; Table S4). Altogether, these data suggest that Rbpms2 functions to promote inclusion of these specific exons into mature transcripts in wild-type embryos.

Despite supporting evidence from differential isoform expression analysis (Figure S8B; Table S3), rMATS did not identify alternative splicing of *pln*, likely because it involves a terminal exon (Figure S9), which rMATS is not designed to evaluate (Figure 3A). Therefore, we employed the Mixture-of-Isoforms algorithm[79] to evaluate alternative splicing of *pln* in *rbpms2*-null animals and found strong statistical evidence that the exon 3-containing *pln*-203 isoform (ENSDART00000141159) is uniquely reduced in mutant animals. Specifically, the Bayes factor was largely above the accepted cutoff of 5 for differences in ENSDART00000141159 versus ENSDART00000133911 usage in wild-type and double-mutant animals across all 5 replicate pairs (Table S5), which is strongly suggestive of differential alternative splicing. This conclusion was also supported by genotype-specific differences in read densities across the locus (Figure S9). Collectively, these data demonstrate that *rbpms2*-null embryos display abnormal splicing of sarcomere and calcium handling genes.

Validation of Differential ASEs in *rbpms2*-Null Zebrafish

Next, we used splicing-sensitive RT-qPCR to validate differential ASEs that were detected by RNA-sequencing.

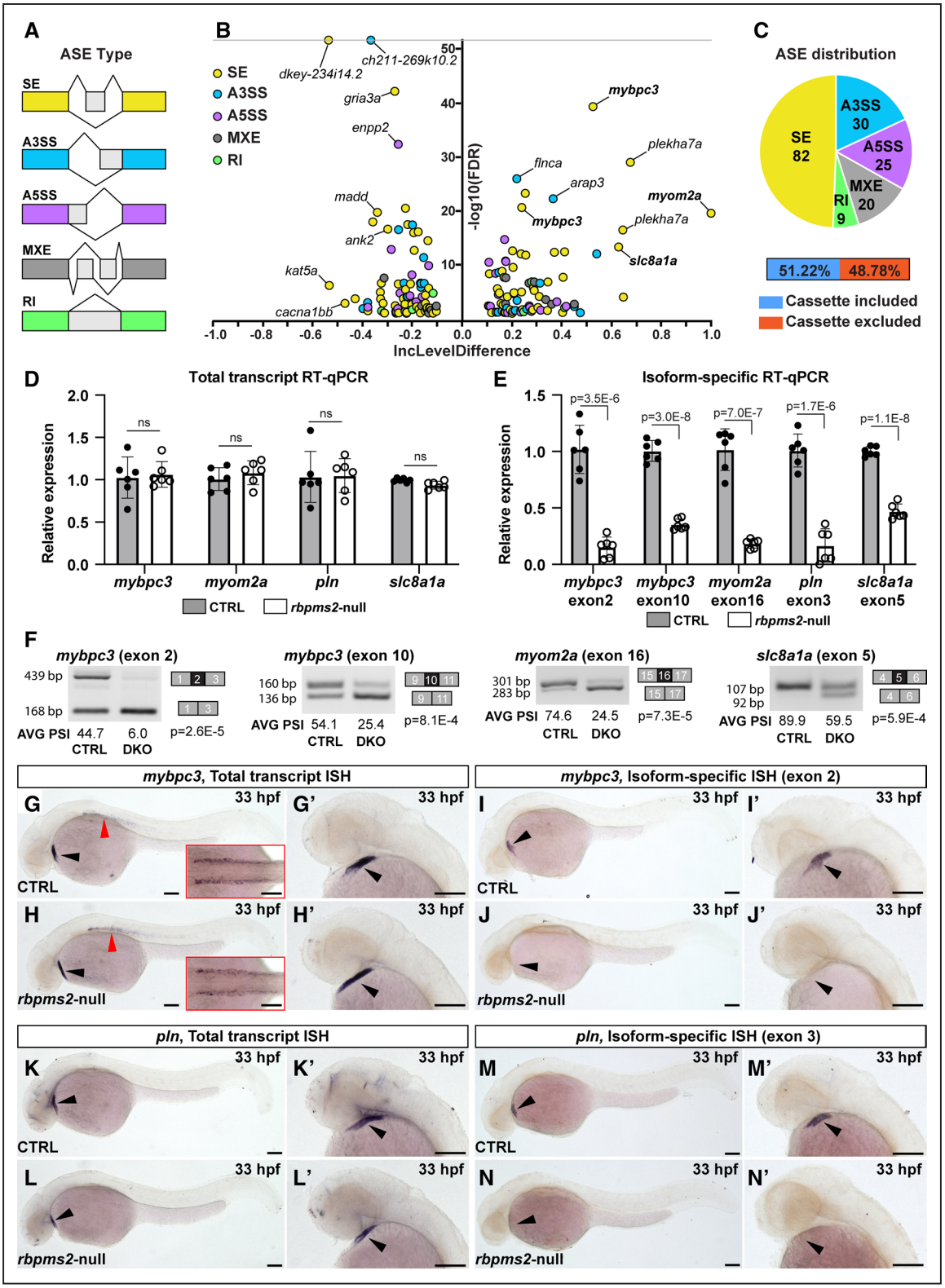

Figure 3. Identification of differential alternative splicing events (ASEs) in *rbpms2*-null embryos.
A, Schematic diagrams of the categories of ASEs investigated by the RNA-sequencing Multivariate Analysis of Transcript Splicing algorithm including skipped exon (SE), alternative 3′ splice site (A3SS), alternative 5′ splice site (A5SS), mutually exclusive exon (MXE), and retained intron (RI). **B**, Volcano plot showing the inclusion (Inc) level differences ($IncLevel^{CTRL}$ – $IncLevel^{rbpms2\text{-}null}$) and false discovery rates (FDRs) for differential ASEs between 33 hours postfertilization (hpf) control-sibling (CTRL; n=4, 10 pooled embryos per replicate) and *rbpms2*-null animals (n=5) filtered by 0 uncalled replicates, FDR<0.1, and |Incleveldifference|>0.1. The ASEs shown in bold were validated with splicing-sensitive quantitative PCR (qPCR) or in situ hybridization. **C**. Pie chart showing the proportions of differential ASEs in each category in *rbpms2*-null animals. (*Continued*)

To that end, we designed 2 primer pairs each for several alternatively spliced transcripts. One pair was designed to measure relative total transcript levels between control-sibling and *rbpms2*-null animals, independent of the alternatively spliced exon (Figure S10A). The other was designed to quantify relative isoform-specific levels by having a primer-binding site contained within the exon showing reduced inclusion in mutants (Figure S10A). Consistent with the RNA-sequencing, for each of the four genes tested (*mybpc3*, *myom2a*, *slc8a1*, and *pln*), total transcript levels were not significantly altered in *rbpms2*-null animals (Figure 3D). However, the specific exon-containing isoforms were reduced by at least 50% in all cases, and by greater than 80% in three cases, demonstrating significant exon exclusion in DKO animals at 33 hpf (Figure 3E). These events were also documented in 48 hpf embryos, ruling out a transient disruption in splicing (Figure S10B and S10C). Exon exclusion was also confirmed independently using semiquantitative reverse-transcription PCR followed by calculations of percent spliced in (Figure 3F; Figure S11). Taken together, these data validate the findings from rMATS and the Mixture-of-Isoforms algorithm and demonstrate that Rbpms2 functions to promote the inclusion of these specific exons into mature transcripts.

To confirm that the DKO splicing abnormalities localize to the myocardium, we performed splicing-sensitive in situ hybridization analysis for 2 genes with *rbpms2*-regulated exons large enough to generate effective exon-specific antisense riboprobes (ie, exon 2 of *mybpc3* and exon 3 of *pln*). In a strategy analogous to the splicing-sensitive RT-qPCR we designed a pair of riboprobes for each gene, one probe to detect total transcript pools of *mybpc3* or *pln*, independent of the alternatively spliced exons (Figure S10A), and the other to detect the isoform-specific cassette exon sequences exclusively (Figure S10A). In control-sibling animals at 33 hpf, total *mybpc3* transcripts were localized to both cardiac and skeletal muscle (Figure 3G and 3G′), and total *pln* transcripts were detected exclusively in the heart (Figure 3K and 3K′). As predicted by the validated RNA-sequencing data (Figure 3D), these expression patterns were unaffected by the loss of *rbpms2* (Figure 3H, 3H′, 3L, and 3L′). By contrast, isoform-specific in situ hybridization localized the *rbpms2*-regulated *mybpc3* and *pln* exons to the hearts of control-sibling animals (Figure 3I, 3I′, 3M, and 3M′), but these exon sequences were undetectable in double-mutant hearts (Figure 3J, 3J′, 3N, and 3N′), confirming that these mis-splicing events are cardiac specific. Taken together, these data implicate *rbpms2* in the positive regulation of exon inclusion for several transcripts in the myocardium of embryonic zebrafish.

For those ASEs validated by RT-qPCR or in situ hybridization (*mybpc3*, *myom2a*, *pln*, and *slc8a1a*), exon exclusion in DKO hearts preserves their open reading frames, leading to the replacement of full-length proteins with those lacking amino acids encoded by the excluded exons (Figure S10A), which are likely to have altered function. In the case of *mybpc3* exon 2, it encodes a domain termed C0, which binds to F-actin and the myosin regulatory light chain.[73] C0 is contained exclusively within the cardiac isoform of myosin binding protein C in higher vertebrates (MYBPC3) but is absent from the skeletal muscle isoforms (MYBPC1 and MYBPC2). Similarly, *mybpc3* exon 10 encodes cardiac-specific amino acids that become phosphorylated by PKA (protein kinase A) in response to β-adrenergic signaling.[80,81] For Myom2a, the short stretch of amino acids absent in DKO animals is of unknown function. For *pln*, excluding exon 3 shortens the protein by 5 amino acids on the C-terminus, which has been shown to decrease SERCA inhibitory activity in vitro.[63] Lastly, the *scl8a1a* exon with reduced inclusion in DKO animals is one (ie, exon E) of 6 conserved exons that are alternatively spliced in higher vertebrates to control the calcium sensitivity of the transporter.[82,83]

Zebrafish *rbpms2*-Null Ventricular Cardiomyocytes Exhibit Myofibrillar Disarray and Calcium Handling Defects

Given the nature of the differential ASEs in *rbpms2*-null animals, we evaluated 48 hpf control-sibling and double-mutant hearts for myofibrillar defects after immunostaining with antibodies that recognize either thin filaments, thick filaments, or Z-disks. For all epitopes, prominent

Figure 3 Continued. Also shown are the percentages of exons in the skipped exon category that are differentially included or excluded in *rbpms2* mutants. **D**, Bar graph showing the relative total transcript levels in 33 hpf CTRL and *rbpms2*-null animals that are independent of the alternatively spliced exons. **E**, Bar graph showing the relative levels of isoform-specific transcripts that contain the indicated Rbpms2-regulated exons in 33 hpf CTRL and *rbpms2*-null animals. In **D** and **E**, single biological replicates (n=6) of 10 pooled embryos, each with 3 technical replicates are shown. Error bars show 1 SD. **F**, Representative gel images of semiquantitative reverse-transcription PCR (RT-PCR) amplicons and the average (AVG) percent spliced in (PSI) values for the indicated alternative splicing events in 33 hpf CTRL and *rbpms2*-null (double knockout [DKO]) animals. Amplicon sizes (in base pairs [bp]; **left**) and identities (**right**) are shown. n=3 biological replicates (see Figure S11), 10 pooled embryos/replicate. For **D**–**F**, Statistical significance was determined by an unpaired, 2-tailed Student's *t* test assuming equal variances with Bonferroni-Dunn correction for multiple comparisons (**D** and **E**). Significant *P* values are shown. **G**–**N**′, Representative brightfield images of 33 hpf CTRL (**G**, **G**′, **I**, **I**′, **K**, **K**′, **M**, and **M**′) and *rbpms2*-null (**H**, **H**′, **J**, **J**′, **L**, **L**′, **N**, and **N**′) embryos processed for in situ hybridization (ISH) with riboprobes that detect total pools (**G**–**H**′, **K**–**L**′) or specific exon-containing mRNA isoforms (**I**–**J**′, **M**–**N**′) of *mybpc3* (**G**–**J**′) or *pln* (**K**–**N**′). The cardiac regions in (**G**, **H**, **I**, **J**, **K**, **L**, **M**, and **N**) are shown at higher zoom in (**G**′, **H**′, **I**′, **J**′, **K**′, **L**′, **M**′, and **N**′). Red arrowheads in (**G** and **H**) highlight expression of *mybpc3* in skeletal muscle, which is shown from a dorsal view in the insets. n=10/group. Black arrowheads highlight the linear heart tube. Scale bars=100 µm. ns indicates not significant.

striations were apparent in control-sibling ventricles (Figure 4A, 4A′, 4C, 4C′, 4E), reflecting tandem arrays of sarcomeres within myofibrils, which themselves are aligned transversely and bundled near the cell cortices. By contrast, despite the detection of the epitopes in DKO ventricles, striations were significantly reduced or absent (Figure 4B, 4B′, 4D, 4D′, 4F), indicative of myofibril disarray. We confirmed that myofibril disorganization was also present at an earlier developmental stage of 33 hpf (Figure S7G through S7H′). This defect appears to be specific to ventricular cardiomyocytes because myofibril organization in atrial cardiomyocytes was grossly unperturbed in DKO embryos (Figure S7I through S7J′). Taken together, these data demonstrate that Rbpms2 activity is required for establishing or maintaining the three-dimensional architecture of myofibrils in ventricular cardiomyocytes of the zebrafish embryo.

We also evaluated *rbpms2*-null hearts for defects in calcium handling by comparing the amplitude and duration of their calcium transients to those in control-sibling hearts. Briefly, control-sibling and mutant hearts were explanted from 48 hpf animals and loaded with the ratiometric calcium-sensitive dye Fura-2. Dual wavelength excitation and high-speed imaging were used to capture the fluctuations in cytosolic calcium occurring throughout the myocardium in control-sibling and mutant hearts over several cardiac cycles. From these images, we measured the amplitude and duration of calcium transients within the atrium and ventricle of each heart. Whereas the atrial values were comparable between control and DKO hearts, (Figure 4G, 4H, 4J through 4L, 4N), the ventricular values were both reduced in double mutant hearts (Figure 4G through 4I; 4K through 4M), demonstrating that Rbpms2 regulates calcium handling in ventricular cardiomyocytes of zebrafish embryos.

Human *RBPMS2*-Null Cardiomyocytes Exhibit Myofibrillar Disarray and Calcium Handling Defects

To determine if the cellular function of RBPMS2 is conserved in human cardiomyocytes, we used CRISPR/Cas9-mediated genome editing to target the *RBPMS2* locus in hiPSCs, which allowed us to generate *RBPMS2*-deficient hiPSC-CMs through directed differentiation. We targeted exon 3, which encodes amino acids within the RRM (Figure S12A), and isolated a clone (*ΔRBPMS2*) carrying a biallelic 2 base pair deletion (Figure S12A). The deletion truncates both the full-length protein and its RRM by ≈70% (Figure 5A; Figure S12B) due to a premature stop codon in the shifted reading frame. RT-qPCR analysis revealed a significant (82%) reduction in *RBPMS2* transcripts in *ΔRBPMS2* hiPSCs (Figure 5B) and hiPSC-CMs (Figure 5C), suggesting that the mutant transcripts are susceptible to non-sense mediated decay. This observation, in combination with the large size of the C-terminal truncation (Figure 5A), strongly suggest that *ΔRBPMS2* cells are devoid of RBPMS2 activity. RNA-sequencing and rMATS analysis (see below) revealed that *ΔRBPMS2* cells express at low abundance, an abnormal RBPMS2 transcript lacking exon 3 (Table S6). Because exon 3 encodes a highly conserved motif in the center of the RRM (Figure S2), the resulting aberrant protein is likely to be unstable and lacking in any biological activity.

To investigate whether *RBPMS2*-null human cardiomyocytes exhibit cellular phenotypes similar to those observed in ventricular cardiomyocytes from *rbpms2*-null zebrafish (Figure 4A through 4F), we analyzed myofibril structure in wild-type and Δ*RBPMS2* hiPSC-CMs by double-immunostaining with antibodies that detect thin filaments or Z-disks. The hallmark striations created by thin filaments, which were readily apparent in control cells (Figure 5D, 5E, and 5G), were almost completely absent in *ΔRBPMS2* hiPSC-CMs (Figure 5H, 5I, and 5K). Moreover, whereas the Z-disks in control cardiomyocytes were prominent, well-defined, and arrayed in tandem (Figure 5D, 5F, and 5G), those in *ΔRBPMS2* hiPSC-CMs were smaller, punctate, and disorganized (Figure 5H, 5J, and 5K). Taken together, these data uncover a conserved role for RBPMS2 in establishing or maintaining myofibril organization in human cardiomyocytes.

Next, we evaluated wild-type and *ΔRBPMS2* hiPSC-CMs for defects in calcium handling. hiPSC-CMs cells were loaded with the calcium-sensitive dye Fluo-4, paced at 1Hz, and imaged by line scanning confocal microscopy to capture intracellular calcium dynamics (Figure 5L and 5M). Similar to ventricular cardiomyocytes from *rbpms2*-null zebrafish, *ΔRBPMS2* hiPSC-CMs exhibited reductions in calcium transient amplitude (Figure 5N) and duration (Figure 5O and 5P). These phenotypes were accompanied by decreases in time-to-peak (Figure 5Q) and maximum upstroke velocity (Figure 5R). Lastly, without pacing, *ΔRBPMS2* hiPSC-CMs contracted at a lower spontaneous beat frequency (Figure 5S). These data demonstrate that human cardiomyocytes rely on RBPMS2 function for optimal calcium handling. Taken together, the overlap in sarcomere and calcium handling phenotypes observed between *rbpms2*-null zebrafish and *ΔRBPMS2* hiPSC-CMs suggest that the cellular function of *RBPMS2* is conserved across vertebrate evolution.

Conservation of an RBPMS2-Regulated Alternative Splicing Network Between Zebrafish and Human Cardiomyocytes

To determine if the molecular function of RBPMS2 as a regulator of alternative splicing is conserved in humans, we performed RNA-sequencing on control and *ΔRBPMS2* hiPSC-CMs followed by rMATS analysis. We identified 2679 differential ASEs in *RBPMS2*-deficient hiPSC-CMs when compared to control cells (0 uncalled

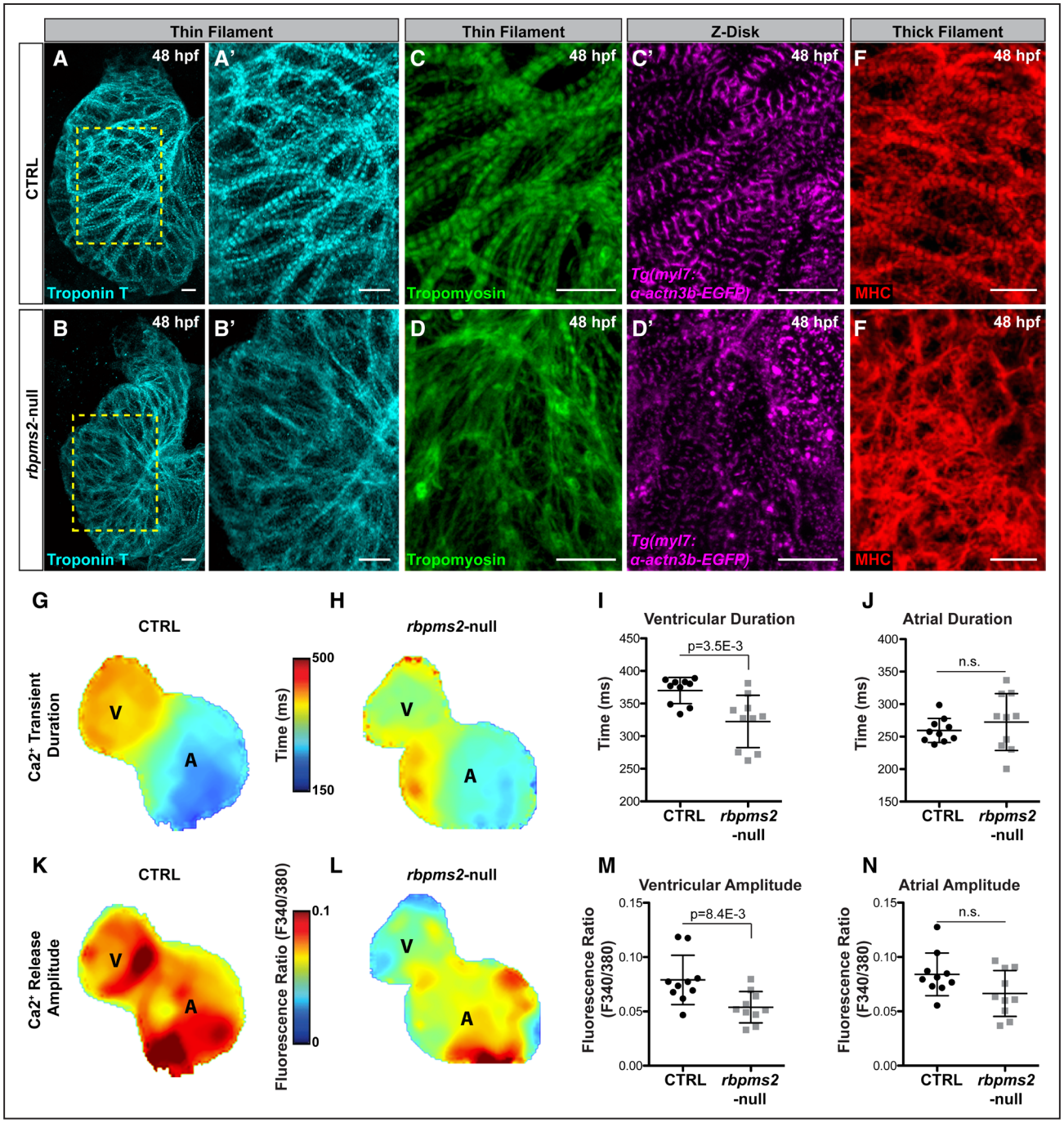

Figure 4. Myofibrillar disarray and calcium handling defects in *rbpms2*-null ventricular cardiomyocytes.
A and **B**′, Representative confocal projections of ventricles in 48 hours postfertilization (hpf) control-sibling (CTRL) or *rbpms2*-null embryos immunostained with an anti-TroponinT antibody (CT3 [cardiac troponin T]) to visualize thin filaments. Regions demarcated in (**A**) and (**B**) are enlarged in (**A**′) and (**B**′). **C** and **D**′′, Confocal projections of ventricles in 48 hpf CTRL and *rbpms2*-null *Tg(α-actn3b-EGFP)* animals coimmunostained with antibodies that detect tropomyosin (CH1; green) to visualize thin filaments or GFP (magenta) to visualize Z-disks. **E** and **F**, Confocal projections of ventricles in 48 hpf CTRL and *rbpms2*-null embryos immunostained with an antibody that detects myosin heavy chain (MF20) to visualize thick filaments. For **A**–**F**, n=10 animals/group. Scale bars=10 μm. **G**–**N**, Color maps (**G**, **H**, **K**, and **L**) and dot plots (**I**, **J**, **M**, and **N**) of calcium transient duration (**G**–**J**) and calcium release amplitude (**K**–**N**) in the ventricle (**G**–**I**; **K**–**M**) and atrium (**G**, **H**, **J**, **K**, **L**, and **N**) of 48 hours postfertilization control-sibling (CTRL; **G**, **I**, **J**, **K**, **M**, and **N**) and *rbpms2*-null (**H**–**J**; **L**–**N**) hearts. Color code depicts localized calcium transient duration in milliseconds (**G** and **H**) or the ratiometric fluorescence indicator of calcium release amplitude (**K** and **L**). Each dot represents center-chamber measurements from one heart. n=10 hearts/group. Error bars show one SD. Statistical significance was determined by an unpaired, 2-tailed Student's *t* test assuming equal variances. Significant *P* values are shown. A indicates atrium; ns, not significant; and V, ventricle.

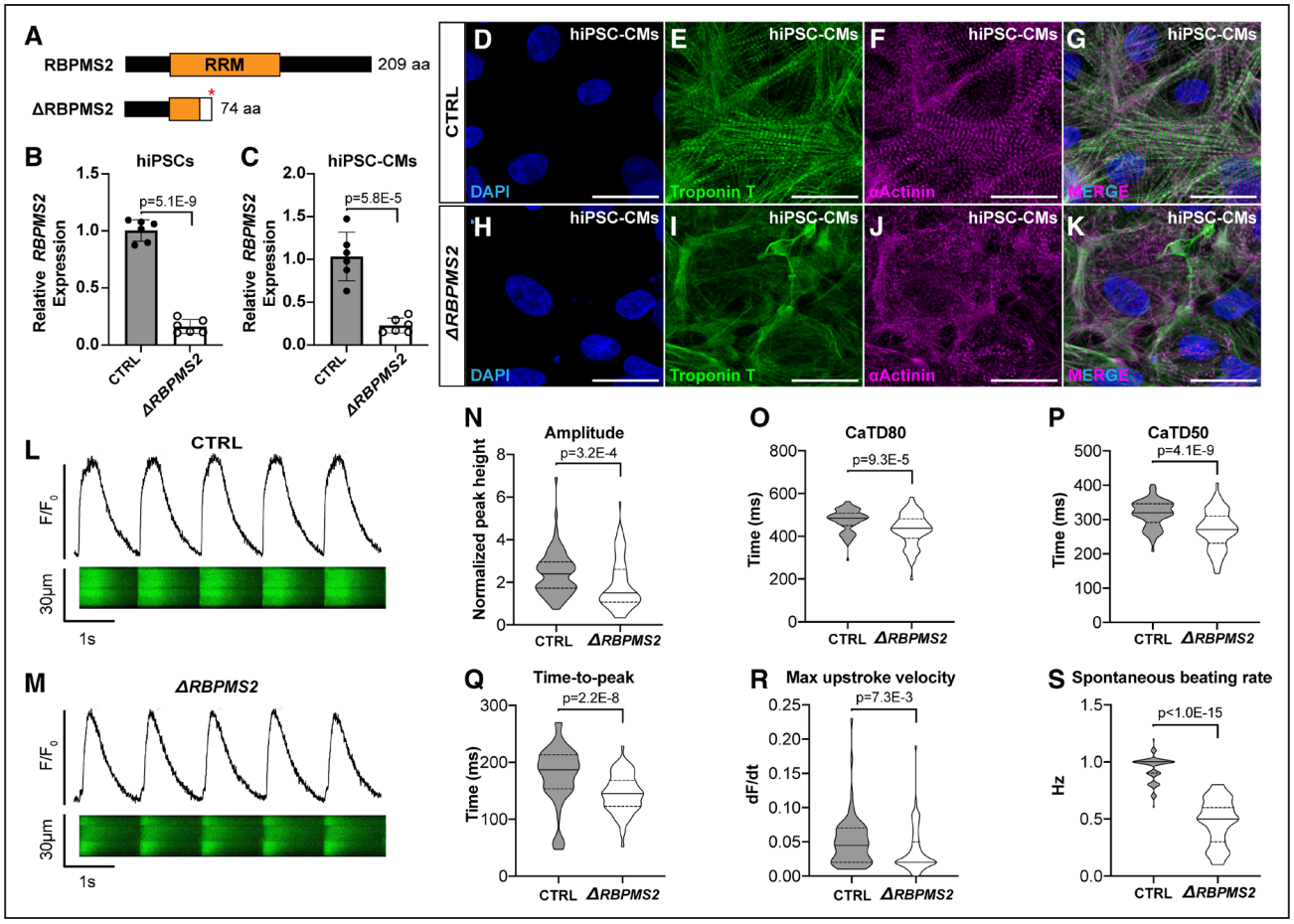

Figure 5. Human *RBPMS2*- (RNA-binding protein with multiple splicing [variants] 2)-null cardiomyocytes exhibit myofibrillar disarray and calcium handling defects similar to those in zebrafish *rbpms2*-null cardiomyocytes.
A, Schematic diagrams of human RBPMS2 (**top**) and the predicted protein product of the Δ*RBPMS2* null allele created with CRISPR/Cas9-mediated genome editing (**bottom**). The asterisk shows the location of a premature stop codon within the RRM (RNA-recognition motifs) caused by a frame-shifting 2 base pair deletion. The white box shows the location of divergent amino acids before the stop codon. **B** and **C**, Bar graphs showing the relative expression levels of *RBPMS2* in wild-type control (CTRL) and Δ*RBPMS2* human induced pluripotent stem cells (hiPSCs; **B**) and cardiomyocytes (hiPSC-CMs; **C**) after 15 days of directed differentiation. n=6 biological replicates/group, each with three technical replicates. Error bars show one standard deviation. Statistical significance was determined by an unpaired, 2-tailed Student's *t* test assuming equal variances. Significant *P* values are shown. **D**–**K**, Representative confocal projections of CTRL (**D**–**G**) and Δ*RBPMS2* (**H**–**K**) hiPSC-CMs immunostained with antibodies that detect cardiac troponin T (CT3; green) or alpha-actinin (anti-sarcomeric alpha-actinin; magenta) to visualize thin filaments or Z-disks, respectively, and counterstained with DAPI (4',6-diamidino-2-phenylindole; blue). Single (**D**–**F**; **H**–**J**) and merged triple (**G** and **K**) channel images are shown. n=50 cells/group from at least 3 wells from 2 separate differentiations. **L** and **M**, Representative traces of fluorescence intensity over baseline (F/F_0; **top**) derived from line scans (**bottom**) of CTRL (**L**) and Δ*RBPMS2* (**M**) hiPSC-CMs loaded with fluo-4 and paced at 1 Hz. **N**–**S**, Violin plots showing calcium transient amplitude (**N**), duration at 80% (CaTD80; **O**) and 50% (CaTD50; **P**) repolarization, time-to-peak amplitude (**Q**), upstroke velocity (**R**), and unpaced spontaneous beating rate (**S**). n=80 cells/group, 40 each from 2 separate differentiations. Statistical significance was determined by an unpaired, 2-tailed Student's *t* test assuming equal variances or a Mann-Whitney *U* test. Significant *P* values are shown. Scale bars=25 μm.

replicates; false discovery rate <0.05; |Incleveldifference|>0.1; Figure 6A; Table S6). A majority (52%) of ASEs were skipped exons, followed by mutually exclusive exons (34%), alternative 3′ splice site (6%), retained intron (4%), and alternative 5′ splice site (4%; Figure 6B; Table S6). Within the skipped exon category, exon exclusion was more frequent than exon inclusion in *RBPMS2*-deficient hiPSC-CMs (Figure 6B; Table S6). GO term enrichment analysis identified overrepresentation of several broad GO terms as well as myofibril, sarcomere, I band, and Z-disc, consistent with the myofibrillar disorganization observed in mutant iPSC-CMs (Table S6).

Lastly, we utilized ExOrthist software[84] to investigate whether a conserved network of genes relies on *RBPMS2*-mediated alternative splicing in both zebrafish and human cardiomyocytes. First, genes harboring Rbpms2-regulated splicing events in zebrafish were compared to those in hiPSC-CMs (Figure 6C). Of the 150 mis-spliced genes in *rbpms2*-null zebrafish, 132 have an ortholog in the human genome, and 29 orthologs were found to harbor RBPMS2-regulated exons in hiPSC-CMs (Figure 6C; Table S7). Next, exon-level analysis identified orthologous exons between the zebrafish and human genomes and determined that of the 166 *rbpms2*-regulated exons

ORIGINAL RESEARCH

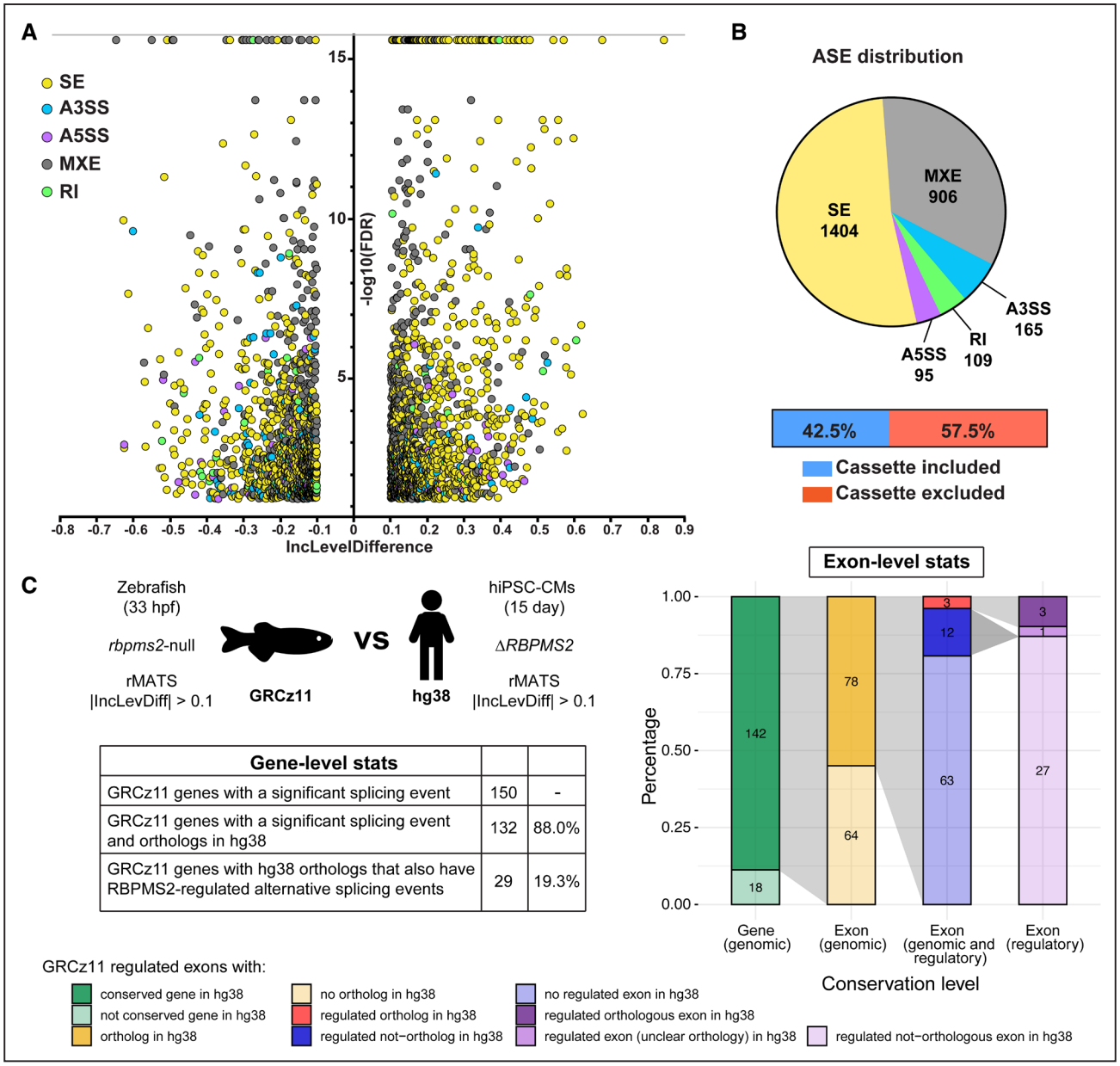

Gene-level stats		
GRCz11 genes with a significant splicing event	150	-
GRCz11 genes with a significant splicing event and orthologs in hg38	132	88.0%
GRCz11 genes with hg38 orthologs that also have RBPMS2-regulated alternative splicing events	29	19.3%

Figure 6. Conservation of RBPMS2 (RNA-binding protein with multiple splicing [variants] 2)-regulated splicing events in zebrafish and human induced pluripotent stem cell–derived cardiomyocytes (hiPSC-CMs).
A, Volcano plot showing the inclusion (Inc) level differences (Inclevel^{CTRL}−InclevelΔ^{RBPMS2}) and false discovery rates (FDRs) for differential alternative splicing events (ASEs) between wild-type control (CTRL; n=4 from independent differentiations) and Δ*RBPMS2* (n=5) filtered by 0 uncalled replicates, FDR<0.05 (capped at 10^{-16}), and |Incleveldifference|>0.1. **B**, Pie chart showing the proportions of differential ASEs in each category in Δ*RBPMS2* hiPSC-CMs. Also shown are the percentages of exons in the skipped exon category that are differentially included or excluded in Δ*RBPMS2* hiPSC-CMs. **C**, Schematic diagram (**left**, **top**), table (**left**, **bottom**), and stacked bar chart (**right**) showing gene- and exon-level comparisons of the splicing defects in *RBPMS2*-deficient zebrafish (GRCz11[genome reference consortium zebrafish build 11]) and hiPSC-CMs (Hg38 [genome reference consortium human build 38]) made by ExOrthist software using the zebrafish ASEs as the query group. Of the 166 differential ASEs, 6 were in low-confidence orthologs (not shown in **C**, **right**). A3SS indicates alternative 3′ splice site; A5SS, alternative 5′ splice site; MXE, mutually exclusive exon; RI, retained intron; rMATS, replicate multivariate analysis of transcript splicing; and SE, skipped exon.

in zebrafish, 142 reside in genes with high-confidence human gene orthologs (Figure 6C). Seventy-eight have an orthologous exon in the corresponding human gene, and three orthologous human exons are regulated by RBPMS2 in hiPSC-CMs (Figure 6C; Table S7). They include exons in *slc8a1a* (see above), *cacnb2a* (calcium voltage-gated channel auxiliary subunit beta 2b), and *ccser2a* (coiled-coil serine-rich protein 2a; Table S7). Cacnb2a is an auxiliary subunit of an L-type voltage-gated calcium channel,[85] and Ccser2a is of unknown function. All in all, despite 450 million years of evolutionary divergence between zebrafish and humans,[86] 31 zebrafish exons are contained within a conserved network of 29 ortholog pairs that rely on RBPMS2 for splicing in

both zebrafish and hiPSC-CMs (Figure 6C; Table S7). In a majority of cases (27/31), orthologous genes are regulated by RBPMS2 through non-orthologous exons (Figure 6C), which is an evolutionary pattern observed for several splicing factors, such as NOVA2 (NOVA alternative splicing regulator 2), CELF, and MBNL.[84,87–89]

DISCUSSION

We report that the RBP RBPMS2 functions as a conserved regulator of alternative splicing, myofibrillar organization, and calcium handling in both zebrafish and human cardiomyocytes. We identified the paralogs *rbpms2a* and *rbpms2b* in a differential expression screen designed to uncover mRNAs enriched in a mixed population of cardiopharyngeal progenitors and cardiomyocytes in the zebrafish ALPM. During zebrafish heart development, Rbpms2 localizes selectively to cardiomyocytes, and cardiomyocyte expression continues into adulthood, which is suggestive of a life-long function in the heart. Cardiomyocyte-enriched expression of *RBPMS2* was previously documented in amphibians, avians, and humans[36,39,41], which is suggestive of functional conservation throughout evolution. Despite these observations and the prior probability that *RBPMS2* is performing a conserved and essential function in cardiomyocytes, this hypothesis had yet to be explored through gene knockout studies.[37]

In a previous study, investigators used morpholinos to knock down expression of the Rbpms2 homolog (ie, *hermes*) in *Xenopus laevis* embryos.[38] Although morphant embryos suffered from cardiac defects, the control morpholino induced a similar phenotype, preventing any conclusions to be drawn. In a reciprocal approach, the authors overexpressed *rbpms2* and documented a reduction in early myocardial gene expression and failure of heart tube formation,[38] suggesting that *rbpms2* serves as a negative regulator of cardiomyocyte differentiation. This function would be consistent with the demonstrated role of *RBPMS2* as a negative regulator of smooth muscle cell differentiation when overexpressed in cells of the avian gastrointestinal tract.[90] If *rbpms2* were acting as a negative regulator of cardiomyocyte differentiation, then *rbpms2*-deficient zebrafish would be predicted to exhibit increased cardiomyocyte numbers, which was not observed. This observation reduces the likelihood that *RBPMS2* serves as a negative regulator of cardiomyocyte differentiation, at least when expressed at physiologic levels.

Instead, our data demonstrate that *RBPMS2* functions on a cellular level to establish or maintain myofibrillar structure in cardiomyocytes. Although *RBPMS2*-deficient zebrafish and human cardiomyocytes express sarcomere proteins, they lack the characteristic striations observed in control cells, which are created by highly ordered, tandem arrays of sarcomeres within myofibrils. The disordered nature of the contractile apparatus in *rbpms2*-deficient zebrafish cardiomyocytes almost certainly explains, at least in part, why DKO hearts show a reduction in ejection fraction.

RBPMS2 also functions in cardiomyocytes to optimize calcium handling as evidenced by reductions in the amplitude and duration of calcium transients in *RBPMS2*-deficient zebrafish and hiPSC-CMs. The dynamics of calcium flux in cardiomyocytes are determined by several interdependent regulatory mechanisms including the activities of calcium channels and transporters, the calcium-binding capacities of intracellular proteins, sarcoplasmic reticulum stores, and baseline cytosolic calcium.[91] As such, pinpointing the primary molecular cause of altered calcium handling in mutant cardiomyocytes will require further investigation. Nonetheless, given the importance of calcium flux in cardiomyocyte physiology, we presume that the documented abnormalities contribute, at least in part, to the functional deficits since reduced calcium transient amplitude and duration are consistent with systolic dysfunction and reduced ejection fraction. Lastly, because mutations in sarcomere components can alter calcium handling[92,93] and calcium handling defects can disrupt myofibrils,[76,77] these phenotypes might be interrelated. Ultimately, the similarities in cellular phenotypes between *RBPMS2*-deficient cardiomyocytes in two species that diverged ≈450 million years ago[86] suggests that the cellular function of RBPMS2 has been conserved. Interestingly, despite *rbpms2* expression in both chambers of the zebrafish heart, the functional, myofibrillar, and calcium handling defects in *rbpms2*-null embryos mutants are largely confined to the ventricle, for unknown reasons.

Our data also demonstrate that *RBPMS2* regulates alternative splicing because numerous differential ASEs were uncovered in *rbpms2*-null zebrafish and *ΔRBPMS2* hiPSC-CMs. In noncardiomyocytes, RBPMS2 regulates the stability, subcellular localization, and translation efficiency of target RNAs (reviewed in Akerberg et al[37]). Despite the observation that amphibian Rbpms2 interacts directly with 2 splicing factors,[94,95] RBPMS2 itself was never implicated in splicing regulation through genetic loss-of-function studies. Notably, the highly related RBPMS protein is a master regulator of alternative splicing in smooth muscle cells,[70] which increased the likelihood that RBPMS2 also regulates alternative splicing in some contexts. Consistent with this possibility, RBPMS2 was capable of substituting for RBPMS in regulating alternative splicing of minigenes containing the RBPMS RNA recognition element,[70] which is also bound by RBPMS2.[96]

Consistent with the observed cellular phenotypes, we documented mis-splicing of genes in *rbpms2*-null zebrafish that encode sarcomere components (Mybpc3 and Myom2a) or proteins that regulate calcium flux in cardiomyocytes (Pln and Slc8a1a). Although we are tempted to draw strong conclusions about how mis-splicing of ≥1 transcripts leads to specific cellular defect, several considerations complicate this task. Because the open reading frames of these four mis-spliced genes remain

intact in DKO zebrafish, the resulting proteins continue to be expressed at normal levels, but without the amino acids encoded by the excluded exons. Therefore, protein activities are likely to be altered, but it is difficult to predict *a priori* how the missing amino acids will affect protein function. Although it is possible that the mutant proteins are completely devoid of activity, in which case the null phenotypes in zebrafish or other model organisms might be informative, it is equally likely that the protein activities are partially reduced, hyperactivated, or altogether new. In an effort to establish causality of the mis-splicing events, one could recapitulate the mis-splicing events by knocking out the excluded exons in wild-type animals or attempt to rescue the mutant phenotype by adding back properly spliced transcripts. Although these approaches might be feasible for 1 or 2 genes at a time, they would be complicated by the likelihood that the cellular phenotypes arise from the combinatorial effects of multiple mis-splicing events, including those we validated (5) and many that we did not (161). For example, although we validated 5 differential ASEs in four myocardial genes, *rbpms2*-null zebrafish embryos also differentially splice *me2* (malic enzyme), *asb5b* (ankyrin repeat and SOCS box containing 5b), *rbfox2*, *plekha7a/hadp1* (pleckstrin homology domain containing family member 7a; Table S4), all of which are also expressed in the zebrafish embryonic myocardium.[97–99] Importantly, our analysis identified a conserved network of 29 ortholog pairs that relies on RBPMS2 for alternative splicing regulation in zebrafish and human cardiomyocytes. This list includes several genes that are integral to heart development or function including *RBFOX2, SLC8A1, and MYBPC3*.[24,75,78] It remains possible that a greater number of ortholog pairs exist but some evaded detection. This could be due to experimental constraints such as having to perform RNA-sequencing on whole embryos rather than isolated hearts.

The goal of ascribing causality of differential ASEs to cellular phenotypes would be aided by the identification of transcriptome-wide Rbpms2 binding sites in wild-type cardiomyocytes using enhanced cross-linking and immunoprecipitation methodology.[100] Unfortunately, this is not feasible in zebrafish embryos because of the difficulty in recovering the large number of purified cardiomyocytes required for analysis (≈20 million per replicate). A priority for future studies will be to identify direct targets of RBPMS2 using either transgenic approaches[101] or enhanced cross-linking and immunoprecipitation analysis of hiPSC-CMs or cardiomyocytes from adult zebrafish.

Although elevated *RBPMS2* expression levels have been detected in gastric cancers[102] and chronic intestinal pseudo-obstruction,[90] mutations in *RBPMS2* have not been implicated in the pathogenesis of human disease to our knowledge. The severity of the myofibrillar defects observed *ΔRBPMS2* hiPSC-CMs suggests that human embryos devoid of *RBPMS2* would suffer from early cardiac dysfunction and potentially embryonic lethality. Accordingly, based on human sequencing data in the Genome Aggregation Database,[103] *RBPMS2* appears to be intolerant to loss-of-function mutations because the observed (o) number of predicted loss-of-function single nucleotide variants is significantly lower than expected (e; gnomAD v2.1.1). Whereas 11.2 predicted loss-of-function single nucleotide variants are predicted, only one has been observed in a heterozygous individual of unknown health. This o/e ratio (0.09) and reported CI (0.03–0.42) suggest that *RBPMS2* is intolerant to mutations in the human population and may be haploinsufficient in most cases.[103] Future studies on hiPSC-CMs heterozygous for *RBPMS2* null alleles will provide important insight regarding the potential haploinsufficiency of this gene.

While this manuscript was in revision, Gan et al[104] reported that the highly related *Rbpms* gene is required for maintaining cardiomyocyte diploidy and enabling cardiomyocyte proliferation during mouse heart development, which protects the heart from noncompaction cardiomyopathy. Over 150 differential ASEs were detected in *Rbpms*-null ventricles, and the cardiac phenotypes were attributed, at least in part, to mis-splicing of the *Pdlim5* gene. Together, the study by Gan et al[104] and the current study highlight species-specific differences between the expression patterns and functions of *Rbpms* and *Rbpms2* in the vertebrate heart. Our study demonstrates that in zebrafish, *rbpms2a* and r*bpms2b* are significantly enriched in cardiomyocytes, and knocking out both genes disrupts embryonic heart function. By contrast, *rbpms* is not enriched in the zebrafish ALPM (Table S1) and does not appear to be expressed in the embryonic heart,[40] which suggests that *rbpms* knockout zebrafish would not exhibit cardiac defects. In the mouse embryo, *Rbpms* expression is significantly enriched in cardiomyocytes,[36,37,104] and knocking it out disrupts heart development.[104] To our knowledge, the developmental expression pattern of *Rbpms2* has not been published,[37] but *Rbpms2* knockout mice did not show cardiac defects at 12 weeks of age.[105] Taken together, these data suggest that *rbpms2* serves an indispensable function in the zebrafish heart, whereas *Rbpms* performs a similarly important function in the mouse heart. It remains possible that *Rbpms2* and *Rbpms* perform semiredundant functions in the mouse heart, which would be revealed if the cardiac phenotype of *Rbpms, Rbpms2* double mutant mice were more severe than *Rbpms*-null animals.

It is difficult to compare and contrast the phenotypes of *rbpms2*-deficient zebrafish and *Rbpms*-deficient mice because of species-specific differences in the heart and because the focus of the Gan et al[104] study differed from ours. Whereas Gan et al[104] evaluated *Rbpms*-deficient mouse hearts for premature cardiomyocyte polyploidization and noncompaction, we evaluated *rbpms2*-deficient zebrafish for abnormalities in sarcomere structure and calcium handling. There is little rationale for evaluating *rbpms2*-deficient zebrafish for premature polyploidization

and noncompaction because, unlike mouse cardiomyocytes, zebrafish cardiomyocytes remain diploid throughout life[44] and trabecular compaction does not occur in zebrafish.[106] In both species, null animals exhibited defects in alternative splicing. It will be informative in future studies to compare the differentially spliced genes in *rbpms2*-deficient zebrafish and *Rbpms*-null mouse hearts to determine how much overlap might exist on a molecular level. Important differences are likely to exist because we did not detect mis-splicing of the *Pdlim5* homologs *pdlim5a* or *pdlim5b* in *rbpms2*-null zebrafish (Table S4).

Knocking out either *RBPMS2* (this study) or *RBPMS*[104] in hiPSC-CMs elicited phenotypes, suggesting that both genes perform important activities in human cardiomyocytes. The degree of phenotypic overlap between *RBPMS2*- and *RBPMS*-null hiPSC-CMs remains unclear because they were examined for different cellular phenotypes in both studies. In future studies, it would be informative to perform a side-by-side comparison of *Rbpms2*-null and *Rbpms*-null hiPSC-CMs, together with double mutant hiPSC-CMs, using the same cellular and molecular assays to determine redundant and non-redundant requirements for these genes in human cardiomyocytes.

We propose a model whereby RBPMS2 regulates alternative splicing of its target genes, many of which are likely to be expressed in multiple tissue lineages, to optimize the activities of the encoded proteins specifically for cardiomyocytes. In the absence of RBPMS2, the resulting differential ASEs either disrupt protein production by shifting the reading frame or lead to the production of proteins with suboptimal activities within cardiomyocytes. These molecular abnormalities are likely to interact in a combinatorial fashion to induce the cardiac phenotype. It remains possible that RBPMS2 also performs splicing-independent functions in regulating the stability, subcellular localization, or translational efficiency of target genes in cardiomyocytes, which would also complicate efforts to ascribe the cardiac phenotype to mis-splicing of individual mRNAs. Future attempts to identify transcriptome-wide binding sites for RBPMS2, coupled with an analysis of how the direct targets behave in mutant animals or cells, will evaluate the possibility of splicing-independent functions for *RBPMS2*. Ultimately, our study and the recent study by Gan et al[104] begin to highlight the important roles played by a novel family of RBPs in the regulation of vertebrate cardiomyocyte physiology.

ARTICLE INFORMATION

Received July 26, 2022; revision received October 27, 2022; accepted November 1, 2022.

Affiliations

Division of Basic and Translational Cardiovascular Research, Department of Cardiology, Boston Children's Hospital, Boston, MA (A.A.A., M.T., X.L., W.T.P., C.E.B., C.G.B.). Cardiovascular Research Center, Massachusetts General Hospital, Charlestown, MA (A.A.A., A.S., L.Z., M.M., S.Y., C.N., C.E.B., C.G.B.). Harvard Medical School, Boston, MA (A.A.A., M.T., A.S., L.Z., M.B., X.L., M.M., S.Y., C.M., C.N., W.T.P., C.E.B., C.G.B.). BioMicroCenter, Department of Biology (V.B.), Department of Biology (V.B., L.B.), and Department of Biological Engineering (L.B.), Massachusetts Institute of Technology, Cambridge, MA. Division of Cardiovascular Medicine, Brigham and Women's Hospital, Boston, MA (M.B., C.M.). Cardiovascular Innovation Research Center, Heart Vascular & Thoracic Institute, Cleveland Clinic, Cleveland, OH (C.N.). Harvard Stem Cell Institute, Cambridge, MA (W.T.P., C.E.B.).

Acknowledgments

Fluorescence-activated cell sorting was performed at the Harvard Stem Cell Institute-Center for Regenerative Medicine Flow Cytometry Core. Customized TALENs (transcription activator-like effector nucleases) were generated by the Broad Institute Genetic Perturbation Platform. Library preparation, RNA-sequencing, and bioinformatics analyses were performed at the MIT BioMicroCenter. Ryan Abo of the MIT BioMicroCenter provided assistance with bioinformatics analysis. Sanger sequencing and DNA-fragment analysis were performed at the Massachusetts General Hospital Computational and Integrative Biology DNA Core.

Sources of Funding

A.A. Akerberg was supported by an American Heart Association (AHA) Postdoctoral Fellowship (20POST35110027). A.A. Akerberg and A. Schwertner were supported by a National Institutes of Health (NIH) training grant awarded to Massachusetts General Hospital (MGH; T32HL007208; Principal Investigator [PI]: A. Rosenzweig). M. Trembley was supported by an NIH training grant awarded to Boston Children's Hospital (T32HL007572; PI: W.T. Pu). S. Yuan was supported by NIH grant 1R01HL165241-01, the Charles Hood Foundation, and AHA grant 940516. L. Boyer was supported by NIH grant R01-HL140471. The bioinformatics analysis was supported in part by the Koch Institute Support (core) Grant P30-CA14051 from the National Cancer Institute. The Burns Laboratory was supported by NIH grants 7R01HL139806 (formerly 1R01HL139806) and 7R35HL135831 (formerly 1R35H135831) to C.G. Burns and C.E. Burns, respectively, by awards from the Executive Committee on Research at MGH to C.G. Burns, and by Department of Defense Peer-Reviewed Medical Research Program (PRMRP) grant W81XWH-20-1-0165 to C.E. Burns. C.E. Burns was a d'Arbelhoff MGH Research Scholar. C.E. Burns and C.G. Burns were Hassenfeld Cardiovascular Scholars at MGH. The Burns Laboratory was supported, in part, by funds from the Boston Children's Hospital Department of Cardiology.

Disclosures

None.

Supplemental Materials

Supplemental Methods
Tables S1–S8
References[107–129]

REFERENCES

1. Fernandez-Jimenez R, Hoit BD, Walsh RA, Fuster V, Ibanez B. Normal physiology of the cardiovascular system. In: Fuster V, editor. *Hurst's The Heart*. 14th ed., McGraw Hill Education; 2017;101–124.
2. Hajjar RJ, Ishikawa K, Thum T. Molecular and cellular biology of the heart. In: Fuster V, editor. *Hurst's The Heart*. 14th ed., 2017; 125–143.
3. Cahill TJ, Ashrafian H, Watkins H. Genetic cardiomyopathies causing heart failure. *Circ Res*. 2013;113:660–675. doi: 10.1161/CIRCRESAHA.113.300282
4. Lee TM, Hsu DT, Kantor P, Towbin JA, Ware SM, Colan SD, Chung WK, Jefferies JL, Rossano JW, Castleberry CD, et al. Pediatric cardiomyopathies. *Circ Res*. 2017;121:855–873. doi: 10.1161/CIRCRESAHA.116.309386
5. Yotti R, Seidman CE, Seidman JG. Advances in the Genetic Basis and Pathogenesis of Sarcomere Cardiomyopathies. *Annu Rev Genom Hum G*. 2019;20:1–25. doi: 10.1146/annurev-genom-083118-015306
6. Guzzo-Merello G, Cobo-Marcos M, Gallego-Delgado M, Garcia-Pavia P. Alcoholic cardiomyopathy. *World J Cardiol*. 2014;6:771–781. doi: 10.4330/wjc.v6.i8.771
7. Volkova M, Russell R. Anthracycline cardiotoxicity: prevalence, pathogenesis and treatment. *Curr Cardiol Rev*. 2011;7:214–20. doi:10.2174/157340311799960645
8. Virani SS, Alonso A, Aparicio HJ, Benjamin EJ, Bittencourt MS, Callaway CW, Carson AP, Chamberlain AM, Cheng S, Delling FN, et al; American Heart Association Council on Epidemiology and Prevention Statistics Committee and Stroke Statistics Subcommittee. Heart disease and stroke

statistics—2021 update: a report from the American Heart Association. *Circulation*. 2021;143:e254–e743. doi: 10.1161/CIR.0000000000000950
9. Hentze MW, Castello A, Schwarzl T, Preiss T. A brave new world of RNA-binding proteins. *Nat Rev Mol Cell Bio*. 2018;19:327–341. doi: 10.1038/nrm.2017.130
10. Gebauer F, Schwarzl T, Valcárcel J, Hentze MW. RNA-binding proteins in human genetic disease. *Nat Rev Genet*. 2021;22:185–198. doi: 10.1038/s41576-020-00302-y
11. Liao Y, Castello A, Fischer B, Leicht S, Föehr S, Frese CK, Ragan C, Kurscheid S, Pagler E, Yang H, et al. The cardiomyocyte RNA-binding proteome: links to intermediary metabolism and heart disease. *Cell Reports*. 2016;16:1456–1469. doi: 10.1016/j.celrep.2016.06.084
12. Riechert E, Kmietczyk V, Stein F, Schwarzl T, Sekaran T, Jürgensen L, Kamuf-Schenk V, Varma E, Hofmann C, Rettel M, et al. Identification of dynamic RNA-binding proteins uncovers a Cpeb4-controlled regulatory cascade during pathological cell growth of cardiomyocytes. *Cell Reports*. 2021;35:109100. doi: 10.1016/j.celrep.2021.109100
13. Baralle FE, Giudice J. Alternative splicing as a regulator of development and tissue identity. *Nat Rev Mol Cell Bio*. 2017;18:437–451. doi:10.1038/nrm.2017.27.
14. Liu J, Kong X, Zhang M, Yang X, Xu X. RNA binding protein 24 deletion disrupts global alternative splicing and causes dilated cardiomyopathy. *Protein & Cell*. 2019;10:405–416. doi: 10.1007/s13238-018-0578-8
15. Lu SH-A, Lee K-Z, Hsu PW-C, Su L-Y, Yeh Y-C, Pan C-Y, Tsai S-Y. Alternative splicing mediated by rna-binding protein RBM24 facilitates cardiac myofibrillogenesis in a differentiation stage-specific manner. *Circ Res*. 2022;130:112–129. doi: 10.1161/CIRCRESAHA.121.320080
16. Poon KL, Tan KT, Wei YY, Ng CP, Colman A, Korzh V, Xu XQ. RNA-binding protein RBM24 is required for sarcomere assembly and heart contractility. *Cardiovasc Res*. 2012;94:418–427. doi: 10.1093/cvr/cvs095
17. Yang J, Hung L-H, Licht T, Kostin S, Looso M, Khrameeva E, Bindereif A, Schneider A, Braun T. RBM24 is a major regulator of muscle-specific alternative splicing. *Dev Cell*. 2014;31:87–99. doi: 10.1016/j.devcel.2014.08.025
18. Chen X, Liu Y, Xu C, Ba L, Liu Z, Li X, Huang J, Simpson E, Gao H, Cao D, et al. QKI is a critical pre-mRNA alternative splicing regulator of cardiac myofibrillogenesis and contractile function. *Nat Commun*. 2021;12:89. doi: 10.1038/s41467-020-20327-5
19. Fenix AM, Miyaoka Y, Bertero A, Blue SM, Spindler MJ, Tan KKB, Perez-Bermejo JA, Chan AH, Mayerl SJ, Nguyen TD, et al. Gain-of-function cardiomyopathic mutations in RBM20 rewire splicing regulation and re-distribute ribonucleoprotein granules within processing bodies. *Nat Commun*. 2021;12:6324. doi: 10.1038/s41467-021-26623-y
20. Guo W, Schafer S, Greaser ML, Radke MH, Liss M, Govindarajan T, Maatz H, Schulz H, Li S, Parrish AM, et al. RBM20, a gene for hereditary cardiomyopathy, regulates titin splicing. *Nat Med*. 2012;18:766–773. doi: 10.1038/nm.2693
21. Maatz H, Jens M, Liss M, Schafer S, Heinig M, Kirchner M, Adami E, Rintisch C, Dauksaite V, Radke MH, et al. RNA-binding protein RBM20 represses splicing to orchestrate cardiac pre-mRNA processing. *J Clin Invest*. 2014;124:3419–3430. doi: 10.1172/JCI74523
22. Schneider JW, Oommen S, Qureshi MY, Goetsch SC, Pease DR, Sundsbak RS, Guo W, Sun M, Sun H, Kuroyanagi H, et al; Wanek Program Preclinical Pipeline. Dysregulated ribonucleoprotein granules promote cardiomyopathy in RBM20 gene-edited pigs. *Nat Med*. 2020;26:1788–1800. doi: 10.1038/s41591-020-1087-x
23. Homsy J, Zaidi S, Shen Y, Ware JS, Samocha KE, Karczewski KJ, DePalma SR, McKean D, Wakimoto H, Gorham J, et al. De novo mutations in congenital heart disease with neurodevelopmental and other congenital anomalies. *Science*. 2015;350:1262–1266. doi: 10.1126/science.aac9396
24. Verma SK, Deshmukh V, Thatcher K, Belanger KK, Rhyner AM, Meng S, et al. RBFOX2 is required for establishing RNA regulatory networks essential for heart development. *Nucleic Acids Res*. 2022;50:2270gkac055–2270gka2286. doi: 10.1093/nar/gkac055
25. Hu J, Wei C, Xue Y, Shao C, Hao Y, Gou L-T, Zhou Y, Zhang J, Ren S, Chen J. RBFox2-miR-34a-Jph2 axis contributes to cardiac decompensation during heart failure. *Proceedings of the National Academy of Sciences*. 2019;116:6172–6180. doi: 10.1073/pnas.1822176116
26. Wei C, Xue Y, Hu J, Banerjee I, Zhang C, Chen B, Banerjee I, Zhang C, Chen B, Li H, et al. Repression of the central splicing regulator RBFox2 is functionally linked to pressure overload-induced heart failure. *Cell reports*. 2015;10:1521–1533. doi: 10.1016/j.celrep.2015.02.013
27. Misra C, Bangru S, Lin F, Lam K, Koenig SN, Lubbers ER, Hedhli J, Murphy NP, Parker DJ, Dobrucki LW, et al. Aberrant expression of a non-muscle rbfox2 isoform triggers cardiac conduction defects in myotonic dystrophy. *Dev Cell*. 2020;52:748–763.e6. doi: 10.1016/j.devcel.2020.01.037
28. Nutter CA, Jaworski EA, Verma SK, Deshmukh V, Wang Q, Botvinnik OB, Lozano MJ, Abass IJ, Ijaz T, Brasier AR, et al. Dysregulation of RBFOX2 is an early event in cardiac pathogenesis of diabetes. *Cell Reports*. 2016;15:2200–2213. doi: 10.1016/j.celrep.2016.05.002
29. Gao C, Ren S, Lee J-H, Qiu J, Chapski DJ, Rau CD, Zhou Y, Abdellatif M, Nakano A, Vondriska TM, et al. RBFox1-mediated RNA splicing regulates cardiac hypertrophy and heart failure. *J Clin Invest*. 2016;126:195–206. doi: 10.1172/JCI84015
30. Dixon DM, Choi J, El-Ghazali A, Park SY, Roos KP, Jordan MC, et al. Loss of muscleblind-like 1 results in cardiac pathology and persistence of embryonic splice isoforms. *Sci Rep-Uk*. 2015;5:9042. doi: 10.1038/srep09042
31. Giudice J, Xia Z, Wang ET, Scavuzzo MA, Ward AJ, Kalsotra A, Wang W, Wehrens XHT, Burge CB, Li W, et al. Alternative splicing regulates vesicular trafficking genes in cardiomyocytes during postnatal heart development. *Nat Commun*. 2014;5:3603–3603. doi: 10.1038/ncomms4603
32. Giudice J, Xia Z, Li W, Cooper TA. Neonatal cardiac dysfunction and transcriptome changes caused by the absence of Celf1. *Sci Rep-Uk*. 2016;6:35550. doi: 10.1038/srep35550
33. Kalsotra A, Xiao X, Ward AJ, Castle JC, Johnson JM, Burge CB, et al. A postnatal switch of CELF and MBNL proteins reprograms alternative splicing in the developing heart. *Proc National Acad Sci*. 2008;105:20333–20338. doi: 10.1073/pnas.0809045105
34. Kalsotra A, Wang K, Li P-F, Cooper TA. MicroRNAs coordinate an alternative splicing network during mouse postnatal heart development. *Gene Dev*. 2010;24:653–658. doi: 10.1101/gad.1894310
35. Wang H, Chen Y, Li X, Chen G, Zhong L, Chen G, et al. Genome-wide analysis of alternative splicing during human heart development. *Sci Rep-Uk*. 2016;6:35520. doi: 10.1038/srep35520
36. Gerber WV, Yatskievych TA, Antin PB, Correia KM, Conlon RA, Krieg PA. The RNA-binding protein gene, hermes, is expressed at high levels in the developing heart. *Mech Dev*. 1999;80:77–86. doi: 10.1016/s0925-4773(98)00195-6
37. Akerberg AA, Burns CE, Burns CG. Exploring the activities of RBPMS proteins in myocardial biology. *Pediatr Cardiol*. 2019;40:1410–1418. doi: 10.1007/s00246-019-02180-6
38. Gerber WV, Vokes SA, Zearfoss NR, Krieg PA. A role for the RNA-binding protein, hermes, in the regulation of heart development. *Dev Biol*. 2002;247:116–126. doi: 10.1006/dbio.2002.0678
39. Wilmore HP, McClive PJ, Smith CA, Sinclair AH. Expression profile of the RNA-binding protein gene hermes during chicken embryonic development. *Dev Dyn*. 2005;233:1045–1051. doi: 10.1002/dvdy.20392
40. Kaufman OH, Lee K, Martin M, Rothhämel S, Marlow FL. rbpms2 functions in Balbiani body architecture and ovary fate. *PLoS Genet*. 2018;14:e1007489. doi: 10.1371/journal.pgen.1007489
41. Karlsson M, Zhang C, Méar L, Zhong W, Digre A, Katona B, Sjöstedt E, Butler L, Odeberg J, Dusart P, et al. A single–cell type transcriptomics map of human tissues. *Sci Adv*. 2021;7:eabh2169. doi: 10.1126/sciadv.abh2169
42. Zhou Y, Cashman TJ, Nevis KR, Obregon P, Carney SA, Liu Y, Gu A, Mosimann C, Sondalle S, Peterson RE, et al. Latent TGF-β binding protein 3 identifies a second heart field in zebrafish. *Nature*. 2011;474:645–648. doi: 10.1038/nature10094
43. Burns CG, Milan DJ, Grande EJ, Rottbauer W, MacRae CA, Fishman MC. High-throughput assay for small molecules that modulate zebrafish embryonic heart rate. *Nat Chem Biol*. 2005;1:263–264. doi: 10.1038/nchembio732
44. González-Rosa JM, Sharpe M, Field D, Soonpaa MH, Field LJ, Burns CE, Burns CG. Myocardial polyploidization creates a barrier to heart regeneration in Zebrafish. *Dev Cell*. 2018;44:433–446.e7. doi: 10.1016/j.devcel.2018.01.021
45. Lin Y-F, Swinburne I, Yelon D. Multiple influences of blood flow on cardiomyocyte hypertrophy in the embryonic zebrafish heart. *Dev Biol*. 2012;362:242–253. doi: 10.1016/j.ydbio.2011.12.005
46. Ma AC, Lee HB, Clark KJ, Ekker SC. High efficiency In Vivo genome engineering with a simplified 15-RVD GoldyTALEN design. *PLoS One*. 2013;8:e65259. doi: 10.1371/journal.pone.0065259
47. Sander JD, Cade L, Khayter C, Reyon D, Peterson RT, Joung JK, Yeh JJ. Targeted gene disruption in somatic zebrafish cells using engineered TALENs. *Nat Biotechnol*. 2011;29:697–698. doi: 10.1038/nbt.1934
48. Sanjana NE, Cong L, Zhou Y, Cunniff MM, Feng G, Zhang F. A transcription activator-like effector toolbox for genome engineering. *Nat Protoc*. 2012;7:171–192. doi: 10.1038/nprot.2011.431

49. Foley JE, Yeh J-RJ, Maeder ML, Reyon D, Sander JD, Peterson RT, Joung JK. Rapid mutation of endogenous zebrafish genes using zinc finger nucleases made by oligomerized pool engineering (OPEN). *PLoS One*. 2009;4:e4348. doi: 10.1371/journal.pone.0004348
50. Wang G, Yang L, Grishin D, Rios X, Ye LY, Hu Y, Li K, Zhang D, Church GM, Pu WT. Efficient, footprint-free human iPSC genome editing by consolidation of Cas9/CRISPR and piggyBac technologies. *Nat Protoc*. 2017;12:88–103. doi: 10.1038/nprot.2016.152
51. Guner-Ataman B, Paffett-Lugassy N, Adams MS, Nevis KR, Jahangiri L, Obregon P, Kikuchi K, Poss KD, Burns CE, Burns CG. Zebrafish second heart field development relies on progenitor specification in anterior lateral plate mesoderm and nkx2.5 function. *Development (Cambridge, England)*. 2013;140:1353–1363. doi: 10.1242/dev.088351
52. Paffett-Lugassy N, Singh R, Nevis KR, Guner-Ataman B, O'Loughlin E, Jahangiri L, Harvey RP, Burns CG, Burns CE. Heart field origin of great vessel precursors relies on nkx2.5-mediated vasculogenesis. *Nat Cell Biol*. 2013;15:1362–1369. doi: 10.1038/ncb2862
53. Schoenebeck JJ, Keegan BR, Yelon D. Vessel and blood specification override cardiac potential in anterior mesoderm. *Dev Cell*. 2007;13:254–267. doi: 10.1016/j.devcel.2007.05.012
54. Serbedzija GN, Chen JN, Fishman MC. Regulation in the heart field of zebrafish. *Development (Cambridge, England)*. 1998;125:1095–1101. doi: 10.1242/dev.125.6.1095
55. Paffett-Lugassy N, Novikov N, Jeffrey S, Abrial M, Guner-Ataman B, Sakthivel S, Burns CE, Burns CG. Unique developmental trajectories and genetic regulation of ventricular and outflow tract progenitors in the zebrafish second heart field. *Development (Cambridge, England)*. 2017;144:4616–4624. doi: 10.1242/dev.153411
56. Yelon D, Horne SA, Stainier DY. Restricted expression of cardiac myosin genes reveals regulated aspects of heart tube assembly in zebrafish. *Dev Biol*. 1999;214:23–37. doi: 10.1006/dbio.1999.9406
57. Hörnberg H, Cioni J-M, Harris WA, Holt CE. Hermes Regulates Axon Sorting in the Optic Tract by Post-Trancriptional Regulation of Neuropilin 1. *J Neurosci*. 2016;36:12697–12706. doi: 10.1523/jneurosci.2400-16.2016
58. Hami D, Grimes AC, Tsai H-J, Kirby ML. Zebrafish cardiac development requires a conserved secondary heart field. *Development (Cambridge, England)*. 2011;138:2389–2398. doi: 10.1242/dev.061473
59. Lazic S, Scott IC. Mef2cb regulates late myocardial cell addition from a second heart field-like population of progenitors in zebrafish. *Dev Biol*. 2011;354:123–33. doi:10.1016/j.ydbio.2011.03.028
60. Pater E de, Clijsters L, Marques SR, Lin Y-F, Garavito-Aguilar ZV, Yelon D, et al. Distinct phases of cardiomyocyte differentiation regulate growth of the zebrafish heart. *Development (Cambridge, England)*. 2009;136:1633–1641. doi: 10.1242/dev.030924
61. Akerberg AA, Burns CE, Burns CG, Nguyen C. Deep learning enables automated volumetric assessments of cardiac function in zebrafish. *Disease Models & Mechanisms*. 2019;12:dmm040188. doi: 10.1242/dmm.040188
62. Patel DA, Lavie CJ, Milani RV, Shah S, Gilliland Y. Clinical implications of left atrial enlargement: a review. *The Ochsner Journal*. 2009;9:191–196.
63. Gorski PA, Trieber CA, Ashrafi G, Young HS. Regulation of the sarcoplasmic reticulum calcium pump by divergent phospholamban isoforms in zebrafish. *J Biol Chem*. 2015;290:6777–6788. doi: 10.1074/jbc.M114.585604
64. Kamel SM, Opbergen CJM van, Koopman CD, Verkerk AO, Boukens BJD, Jonge B de, et al. Istaroxime treatment ameliorates calcium dysregulation in a zebrafish model of phospholamban R14del cardiomyopathy. *Nat Commun*. 2021;12:7151. doi: 10.1038/s41467-021-27461-8
65. Berdougo E, Coleman H, Lee DH, Stainier DYR, Yelon D. Mutation of weak atrium/atrial myosin heavy chain disrupts atrial function and influences ventricular morphogenesis in zebrafish. *Development (Cambridge, England)*. 2003;130:6121–6129. doi: 10.1242/dev.00838
66. Becker JR, Robinson TY, Sachidanandan C, Kelly AE, Coy S, Peterson RT, MacRae CA. In vivo natriuretic peptide reporter assay identifies chemical modifiers of hypertrophic cardiomyopathy signalling. *Cardiovasc Res*. 2012;93:463–470. doi: 10.1093/cvr/cvr350
67. Grassini DR, Lagendijk AK, Angelis JED, Silva JD, Jeanes A, Zettler N, Bower NI, Hogan BM, Smith KA. Nppa and Nppb act redundantly during zebrafish cardiac development to confine AVC marker expression and reduce cardiac jelly volume. *Development (Cambridge, England)*. 2018;145:dev160739. doi: 10.1242/dev.160739
68. Schmitt JP, Kamisago M, Asahi M, Li GH, Ahmad F, Mende U, Kranias EG, MacLennan DH, Seidman JG, Seidman CE. Dilated cardiomyopathy and heart failure caused by a mutation in phospholamban. *Science*. 2003;299:1410–1413. doi: 10.1126/science.1081578
69. Cunningham F, Allen JE, Allen J, Alvarez-Jarreta J, Amode MR, Armean IM. Ensembl 2022. *Nucleic Acids Res*. 2021;50:D988–D995. doi: 10.1093/nar/gkab1049
70. Nakagaki-Silva EE, Gooding C, Llorian M, Jacob AG, Richards F, Buckroyd A, Sinha S, Smith CW. Identification of RBPMS as a mammalian smooth muscle master splicing regulator via proximity of its gene with super-enhancers. *ELife*. 2019;8:e46327 doi: 10.7554/elife.46327
71. Shen S, Park JW, Lu Z, Lin L, Henry MD, Wu YN, Zhou Q, Xing Y. rMATS: robust and flexible detection of differential alternative splicing from replicate RNA-Seq data. *Proc Natl Acad Sci USA*. 2014;111:E5593–E5601. doi: 10.1073/pnas.1419161111
72. Chen Y-H, Pai C-W, Huang S-W, Chang S-N, Lin L-Y, Chiang F-T, Lin JL, Hwang JJ, Tsai CT. Inactivation of Myosin binding protein C homolog in zebrafish as a model for human cardiac hypertrophy and diastolic dysfunction. *J Am Heart Assoc*. 2013;2:e000231. doi: 10.1161/jaha.113.000231
73. Sadayappan S, de Tombe PP. Cardiac myosin binding protein-C: redefining its structure and function. *Biophysical Reviews* 2012;4:93–106. doi:10.1007/s12551-012-0067-x
74. Tskhovrebova L, Trinick J. Making muscle elastic: the structural basis of myomesin stretching. *Plos Biol*. 2012;10:e1001264. doi:10.1371/journal.pbio.1001264
75. Carrier L, Mearini G, Stathopoulou K, Cuello F. Cardiac myosin-binding protein C (MYBPC3) in cardiac pathophysiology. *Gene*. 2015;573:188–197. doi: 10.1016/j.gene.2015.09.008
76. Ebert AM, Hume GL, Warren KS, Cook NP, Burns CG, Mohideen MA, Siegal G, Yelon D, Fishman MC, Garrity DM. Calcium extrusion is critical for cardiac morphogenesis and rhythm in embryonic zebrafish hearts. *Proc Natl Acad Sci USA*. 2005;102:17705–17710. doi: 10.1073/pnas.0502683102
77. Langenbacher AD, Dong Y, Shu X, Choi J, Nicoll DA, Goldhaber JI, et al. Mutation in sodium–calcium exchanger 1 (NCX1) causes cardiac fibrillation in zebrafish. *P Natl Acad Sci Usa*. 2005;102:17699–17704. doi: 10.1073/pnas.0502679102
78. Ottolia M, John S, Hazan A, Goldhaber JI. The cardiac Na+-Ca+ exchanger: from structure to function. *Compr Physiol*. 2021;12:2681–2717. doi: 10.1002/cphy.c200031
79. Katz Y, Wang ET, Airoldi EM, Burge CB. Analysis and design of RNA sequencing experiments for identifying isoform regulation. *Nat Methods*. 2010;7:1009–1015. doi: 10.1038/nmeth.1528
80. Gautel M, Zuffardi O, Freiburg A, Labeit S. Phosphorylation switches specific for the cardiac isoform of myosin binding protein-C: a modulator of cardiac contraction?. *EMBO J*. 1995;14:1952–1960. doi: 10.1002/j.1460-2075.1995.tb07187.x
81. Mohamed AS, Dignam JD, Schlender KK. Cardiac myosin-binding protein C (MyBP-C): identification of protein kinase a and protein kinase c phosphorylation sites. *Arch Biochem Biophys*. 1998;358:313–319. doi: 10.1006/abbi.1998.0857
82. Quednau BD, Nicoll DA, Philipson KD. Tissue specificity and alternative splicing of the Na+/Ca2+ exchanger isoforms NCX1, NCX2, and NCX3 in rat. *Am J Physiol*. 1997;272:C1250–C1261. doi: 10.1152/ajpcell.1997.272.4.c1250
83. Kofuji P, Lederer WJ, Schulze DH. Mutually exclusive and cassette exons underlie alternatively spliced isoforms of the Na/Ca exchanger. *J Biol Chem*. 1994;269:5145–5149. doi: 10.1016/s0021-9258(17)37667-6
84. Márquez Y, Mantica F, Cozzuto L, Burguera D, Hermoso-Pulido A, Ponomarenko J, Roy SW, Irimia M. ExOrthist: a tool to infer exon orthologies at any evolutionary distance. *Genome Biol*. 2021;22:239. doi: 10.1186/s13059-021-02441-9
85. Zhang Q, Chen J, Qin Y, Wang J, Zhou L. Mutations in voltage-gated L-type calcium channel: implications in cardiac arrhythmia. *Channels*. 2018;12:201–218. doi: 10.1080/19336950.2018.1499368
86. Kumar S, Hedges SB. A molecular timescale for vertebrate evolution. *Nature*. 1998;392:917–20. doi:10.1038/31927
87. Burguera D, Marquez Y, Racioppi C, Permanyer J, Torres-Méndez A, Esposito R, Albuixech-Crespo B, Fanlo L, D'Agostino Y, Gohr A, et al. Evolutionary recruitment of flexible Esrp-dependent splicing programs into diverse embryonic morphogenetic processes. *Nat Commun*. 2017;8:1799. doi: 10.1038/s41467-017-01961-y
88. Irimia M, Denuc A, Burguera D, Somorjai I, Martín-Durán JM, Genikhovich G, et al. Stepwise assembly of the Nova-regulated alternative splicing network in the vertebrate brain. *Proc National Acad Sci*. 2011;108:5319–5324. doi: 10.1073/pnas.1012333108
89. Solana J, Irimia M, Ayoub S, Orejuela MR, Zywitza V, Jens M, Tapial J, Ray D, Morris Q, Hughes TR, et al. Conserved functional antagonism of CELF and MBNL proteins controls stem cell-specific alternative splicing in planarians. *Elife*. 2016;5:e16797. doi: 10.7554/eLife.16797

90. Notarnicola C, Rouleau C, Guen LL, Virsolvy A, Richard S, Faure S, et al. The RNA-binding protein rbpms2 regulates development of gastrointestinal smooth muscle. *Gastroenterology*. 2012;143:687–697.e9. doi: 10.1053/j.gastro.2012.05.047
91. Fearnley CJ, Roderick HL, Bootman MD. Calcium signaling in cardiac myocytes. *Csh Perspect Biol*. 2011;3:a004242–a004242. doi: 10.1101/cshperspect.a004242
92. Fatkin D, McConnell BK, Mudd JO, Semsarian C, Moskowitz IGP, Schoen FJ, Giewat M, Seidman CE, Seidman JG. An abnormal Ca2+ response in mutant sarcomere protein–mediated familial hypertrophic cardiomyopathy. *J Clin Invest*. 2000;106:1351–1359. doi: 10.1172/JCI11093
93. Fraysse B, Weinberger F, Bardswell SC, Cuello F, Vignier N, Geertz B, Starbatty J, Krämer E, Coirault C, Eschenhagen T, et al. Increased myofilament Ca2+ sensitivity and diastolic dysfunction as early consequences of Mybpc3 mutation in heterozygous knock-in mice. *J Mol Cell Cardiol*. 2012;52:1299–1307. doi: 10.1016/j.yjmcc.2012.03.009
94. Nijjar S, Woodland HR. Protein interactions in Xenopus germ plasm RNP particles. *PLoS One*. 2013;8:e80077. doi: 10.1371/journal.pone.0080077
95. Sagnol S, Marchal S, Yang Y, Allemand F, Barbara P de S. Epithelial Splicing Regulatory Protein 1 (ESRP1) is a new regulator of stomach smooth muscle development and plasticity. *Dev Biol*. 2016;414:207–218. doi: 10.1016/j.ydbio.2016.04.015
96. Farazi TA, Leonhardt CS, Mukherjee N, Mihailovic A, Li S, Max KEA, Meyer C, Yamaji M, Cekan P, Jacobs NC, et al. Identification of the RNA recognition element of the RBPMS family of RNA-binding proteins and their transcriptome-wide mRNA targets. *RNA (New York, NY)*. 2014;20:1090–1102. doi: 10.1261/rna.045005.114
97. Ruzicka L, Bradford YM, Frazer K, Howe DG, Paddock H, Ramachandran S, et al. ZFIN. *The zebrafish model organism database: Updates and new directions. Genesis (New York, NY: 2000)*. 2015;53:498–509. doi: 10.1002/dvg.22868
98. Huang M, Akerberg AA, Zhang X, Yoon H, Joshi S, Harding C, et al. Intrinsic myocardial defects underlie an Rbfox deficient zebrafish model of hypoplastic left heart syndrome. *Nat Commun*. 2022;13:5877. doi: 10.1038/s41467-022-32982-x
99. Wythe JD, Jurynec MJ, Urness LD, Jones CA, Sabeh MK, Werdich AA, Sato M, Yost HJ, Grunwald DJ, Macrae CA, et al. Hadp1, a newly identified pleckstrin homology domain protein, is required for cardiac contractility in zebrafish. *Dis Model Mech*. 2011;4:607–621. doi: 10.1242/dmm.002204
100. Nostrand ELV, Pratt GA, Shishkin AA, Gelboin-Burkhart C, Fang MY, Sundararaman B, et al. Robust transcriptome-wide discovery of RNA-binding protein binding sites with enhanced CLIP (eCLIP). *Nat Methods*. 2016;13:508–514. doi: 10.1038/nmeth.3810
101. Rahman R, Xu W, Jin H, Rosbash M. Identification of RNA-binding protein targets with HyperTRIBE. *Nat Protoc*. 2018;13:1829–1849. doi: 10.1038/s41596-018-0020-y
102. Hapkova I, Skarda J, Rouleau C, Thys A, Notarnicola C, Janikova M, Bernex F, Rypka M, Vanderwinden J-M, Faure S, et al. High expression of the RNA-binding protein RBPMS2 in gastrointestinal stromal tumors. *Exp Mol Pathol*. 2013;94:314–321. doi: 10.1016/j.yexmp.2012.12.004
103. Karczewski KJ, Francioli LC, Tiao G, Cummings BB, Alföldi J, Wang Q, Collins RL, Laricchia KM, Ganna A, Birnbaum DP, et al; Genome Aggregation Database Consortium. The mutational constraint spectrum quantified from variation in 141,456 humans. *Nature*. 2020;581:434–443. doi: 10.1038/s41586-020-2308-7
104. Gan P, Wang Z, Morales MG, Zhang Y, Bassel-Duby R, Liu N, Olson EN. RBPMS is an RNA-binding protein that mediates cardiomyocyte binucleation and cardiovascular development. *Dev Cell*. 2022;57:959–973.e7. doi: 10.1016/j.devcel.2022.03.017
105. Spielmann N, Miller G, Oprea TI, Hsu C-W, Fobo G, Frishman G, et al. Extensive identification of genes involved in congenital and structural heart disorders and cardiomyopathy. *Nat Cardiovasc Res*. 2022;1:157–173. doi: 10.1038/s44161-022-00018-8
106. Hu N, Yost HJ, Clark EB. Cardiac morphology and blood pressure in the adult zebrafish. *The Anatomical Record*. 2001;264:1–12. doi: 10.1002/ar.1111
107. Quinlan AR, Hall IM. BEDTools: a flexible suite of utilities for comparing genomic features. *Bioinformatics*. 2010;26:841–2. doi:10.1093/bioinformatics/btq033
108. Patro R, Duggal G, Love MI, Irizarry RA, Kingsford C. Salmon provides fast and bias-aware quantification of transcript expression. *Nat Methods*. 2017;14:417–419. doi: 10.1038/nmeth.4197
109. Soneson C, Love MI, Robinson MD. Differential analyses for RNA-seq: transcript-level estimates improve gene-level inferences. *F1000research*. 2016;4:1521. doi: 10.12688/f1000research.7563.2
110. Dobin A, Davis CA, Schlesinger F, Drenkow J, Zaleski C, Jha S, Batut P, Chaisson M, Gingeras TR. STAR: ultrafast universal RNA-seq aligner. *Bioinformatics*. 2013;29:15–21. doi: 10.1093/bioinformatics/bts635
111. Li B, Dewey CN. RSEM: accurate transcript quantification from RNA-Seq data with or without a reference genome. *BMC Bioinf*. 2011;12:323. doi: 10.1186/1471-2105-12-323
112. Love MI, Huber W, Anders S. Moderated estimation of fold change and dispersion for RNA-seq data with DESeq2. *Genome Biol*. 2014;15:550. doi: 10.1186/s13059-014-0550-8
113. Katz Y, Wang ET, Silterra J, Schwartz S, Wong B, Thorvaldsdóttir H, Robinson JT, Mesirov JP, Airoldi EM, Burge CB. Quantitative visualization of alternative exon expression from RNA-seq data. *Bioinformatics*. 2015;31:2400–2402. doi: 10.1093/bioinformatics/btv034
114. Thisse C, Thisse B. High-resolution in situ hybridization to whole-mount zebrafish embryos. *Nat Protocols*. 2008;3:59–69. doi: 10.1038/nprot.2007.514
115. Schneider CA, Rasband WS, Eliceiri KW. NIH Image to ImageJ: 25 years of image analysis. *Nat Methods*. 2012;9:671–675. doi: 10.1038/nmeth.2089
116. Jahangiri L, Sharpe M, Novikov N, González-Rosa JM, Borikova A, Nevis K, Paffett-Lugassy N, Zhao L, Adams M, Guner-Ataman B, et al. The AP-1 transcription factor component Fosl2 potentiates the rate of myocardial differentiation from the zebrafish second heart field. *Development*. 2016;143:113–122. doi: 10.1242/dev.126136
117. Poss KD, Wilson LG, Keating MT. Heart Regeneration in Zebrafish. *Science*. 2002;298:2188–2190. doi: 10.1126/science.1077857
118. Akerberg AA, Henner A, Stewart S, Stankunas K. Histone demethylases Kdm6ba and Kdm6bb redundantly promote cardiomyocyte proliferation during zebrafish heart ventricle maturation. *Dev Biol*. 2017;426:84–96. doi: 10.1016/j.ydbio.2017.03.030
119. Huisken J, Stainier DYR. Even fluorescence excitation by multidirectional selective plane illumination microscopy (mSPIM). *Opt Lett*. 2007;32:2608–2610. doi: 10.1364/ol.32.002608
120. Power RM, Huisken J. A guide to light-sheet fluorescence microscopy for multiscale imaging. *Nat Methods*. 2017;14:360–373. doi: 10.1038/nmeth.4224
121. Livak KJ, Schmittgen TD. Analysis of relative gene expression data using real-time quantitative PCR and the 2(-Delta Delta C(T)) Method. *Methods (San Diego, Calif)*. 2001;25:402–408. doi: 10.1006/meth.2001.1262
122. Schindelin J, Arganda-Carreras I, Frise E, Kaynig V, Longair M, Pietzsch T, Preibisch S, Rueden C, Saalfeld S, Schmid B, et al. Fiji: an open-source platform for biological-image analysis. *Nat Methods*. 2012;9:676–682. doi: 10.1038/nmeth.2019
123. Panáková D, Werdich AA, MacRae CA. Wnt11 patterns a myocardial electrical gradient through regulation of the L-type Ca(2+) channel. *Nature*. 2010;466:874–878. doi: 10.1038/nature09249
124. Huang DW, Sherman BT, Tan Q, Collins JR, Alvord WG, Roayaei J, Stephens R, Baseler MW, Lane HC, Lempicki RA. The DAVID gene functional classification tool: a novel biological module-centric algorithm to functionally analyze large gene lists. *Genome Biol*. 2007;8:R183–R183. doi: 10.1186/gb-2007-8-9-r183
125. Kanehisa M, Goto S. KEGG: kyoto encyclopedia of genes and genomes. *Nucleic Acids Res*. 2000;28:27–30. doi: 10.1093/nar/28.1.27
126. Nishimura D. BioCarta. Biotechnology Software and Internet Report. 2001;2:117–120. doi: 10.1089/152791601750294344
127. Bastian FB, Roux J, Niknejad A, Comte A, Fonseca Costa SS, de Farias TM, Moretti S, Parmentier G, De Laval VR, Rosikiewicz M, et al. The Bgee suite: integrated curated expression atlas and comparative transcriptomics in animals. *Nucleic Acids Res*. 2020;49:D831–D847. doi: 10.1093/nar/gkaa793
128. Bradford YM, Slyke CEV, Ruzicka L, Singer A, Eagle A, Fashena D, Howe DG, Frazer K, Martin R, Paddock H, et al. Zebrafish information network, the knowledgebase for Danio rerio research. *Genetics*. 2022;220:iyac016. doi: 10.1093/genetics/iyac016
129. Kettleborough RNW, Busch-Nentwich EM, Harvey SA, Dooley CM, de Bruijn E,van Eeden F, Sealy I, White RJ, Herd C, Nijman IJ, et al. A systematic genome-wide analysis of zebrafish protein-coding gene function. *Nature*. 2013;496:494–497. doi: 10.1038/nature11992